Palaeontologia Electronica
palaeo-electronica.org

High local variability in elevation of the Oldman-Dinosaur Park Formation contact revealed by digital outcrop reconstruction, and implications for dinosaur biostratigraphy of the Late Cretaceous (Campanian) Belly River Group of Alberta, Canada

Alexandre V. Demers-Potvin and Hans C.E. Larsson

ABSTRACT

The Late Cretaceous (Campanian) Belly River Group of Dinosaur Provincial Park (DPP), Alberta, Canada, combines the world's most complete dinosaur chronofauna with precise and accurate absolute age constraints obtained from ashfall deposits. However, the time-averaging of individual fossil quarries caused by their preservation in fluvio-deltaic depositional environments implies significant uncertainties on their relative age and by extension on our knowledge of local palaeodiversity patterns. The biostratigraphic position of a multigeneric bonebed at a transitional period between successive dinosaur assemblage zones, combined with its proximity to an exposure of the Oldman-Dinosaur Park Formation (OF-DPF) contact, provides an ideal study system for such an investigation. Images acquired with an unmanned aerial vehicle (UAV) were aligned by structure-from-motion (SfM) photogrammetry to construct a 3-D digital outcrop model (DOM), a digital elevation model (DEM), and an orthomosaic of the 0.446 km^2 area surrounding the bonebed. The first key result is that the absolute elevation of the OF-DPF contact varies by ~12 m locally, which causes hitherto underestimated uncertainties on any fossil locality's stratigraphic height relative to it. Moreover, we find that the lower DPF has the potential to be locally subdivided into at least three successive channel cut-and-fill rhythms, some of which are promising candidate marker beds for a more expansive correlation of DPP's fossil heritage. This study shows how rapidly developing UAV-based geological mapping methods contribute to exploring stratigraphic successions in other fossil-rich regions on a larger scale than what is currently possible from ground-based surveys alone.

Final citation: Demers-Potvin, Alexandre V. and Larsson, Hans C.E. 2025. High local variability in elevation of the Oldman-Dinosaur Park Formation contact revealed by digital outcrop reconstruction, and implications for dinosaur biostratigraphy of the Late Cretaceous (Campanian) Belly River Group of Alberta, Canada. Palaeontologia Electronica, 28(1):a13.
https://doi.org/10.26879/1447
palaeo-electronica.org/content/2025/5473-dinosaur-park-bonebed-3d-model

Alexandre V. Demers-Potvin. Department of Bioengineering and Redpath Museum, McGill University, Montréal, Québec, Canada; alexandre.demers-potvin@mail.mcgill.ca
Hans C.E. Larsson. Department of Biology and Redpath Museum, McGill University, Montréal, Québec, Canada; hans.ce.larsson@mcgill.ca

Keywords: Late Cretaceous; dinosaur; Dinosaur Park Formation; photogrammetry; 3-D model; bonebed

Submission: 9 September 2024. Acceptance: 28 February 2025.

INTRODUCTION

The late Campanian exposures of the Belly River Group (BRG) (Eberth and Hamblin, 1993; Hamblin and Abrahamson, 1996) cropping out along the Red Deer River in Dinosaur Provincial Park (DPP), Alberta, Canada, have preserved one of the most intensely studied Mesozoic non-marine ecosystems following more than a century of sustained geological and palaeontological exploration (Sternberg, 1917; Sternberg, 1950; Russell, 1966; Béland and Russell, 1978; Currie and Koppelhus, 2005 and papers therein). Consequently, the DPP palaeocommunity is now widely accepted to have undergone biotic turnover in the occurrence and abundance of several constituent vertebrate species and families, in coincidence with a gradual marine incursion recorded in sedimentary facies extending over a ~100 m stratigraphic height which is known to represent ~2.429 ± 0.024 Ma based on the latest U-Pb geochronology (Thomas et al., 1990; Ramezani et al., 2022; Brinkman, 1990; Brinkman et al., 1998; Eberth, 2005; Cullen et al., 2021; Eberth et al., 2023). These faunal turnover patterns rest on stratigraphic ranges derived from a database of precise geographical coordinates for more than 650 bonebeds and individual skeleton quarries (to date) distributed over ~80 km^2 of outcrop in and around DPP (Currie and Koppelhus, 2005; Currie and Russell, 2005; Figure 1A). In summary, Dinosaur Provincial Park may preserve one of the world's most promising palaeobiotas in the distant geological past to investigate biotic responses to a sea level rise with highly robust geographical and temporal constraints relative to comparable non-marine fossil localities in deep time.

However, it can be argued that our knowledge of the ecological trends of the DPP palaeobiota remains clouded to a certain extent by underresolved stratigraphic controls. Notably, all of these sites' stratigraphic positions have been estimated solely from their height relative to the nearest measured location of the Oldman Formation - Dinosaur Park Formation (OF-DPF) contact on an isopach map of the Park (Brinkman, 1990; Eberth, 2005; Cullen et al., 2021), while scarcely considering their local sedimentological setting beyond taphonomic significance (Dodson, 1971; Wood et al., 1988; Eberth, 1990, 2015; Ryan et al., 2001; Eberth and Currie, 2005). One of the consequences of this method is that the BRG in DPP (including the OF and DPF) is now frequently partitioned into four successive megaherbivorous dinosaur assemblage zones which collectively form a possible chronofauna (Ryan and Evans, 2005; Mallon et al., 2012; Mallon, 2019; Lowi-Merri and Evans, 2020). Each of these zones has an estimated duration varying between ~650 and ~700 ka based on interpolated rock accumulation rates between radioisotopically dated bentonite beds (Ramezani et al., 2022; Eberth et al., 2023), yet these rates currently do not account for vertical variation in lithological facies (e.g., between sandy channel and muddy overbank deposits) which prevails in DPP's fluvio-deltaic deposits. In other words, the relative heights of DPP's quarries have been assumed to be accurate proxies of relative age even though they have never been successfully correlated in any lithostratigraphic sense over large distances. Moreover, the OF-DPF contact has been assumed to be a relatively consistent horizontal reference datum for measuring stratigraphic positions for more than 30 years (Eberth, 1990; Eberth and Hamblin, 1993). However, its mean absolute elevation varies by around 30 m along a ~20 km east-west gradient across DPP and appears to fluctuate substantially on a more local spatial scale (Figure 1B).

The current lack of lithostratigraphic correlation for DPP as a whole is usually attributed to the frequent down-cutting of muddy overbank deposits by overlying sandy point bar or thalweg deposits, which is a common feature of fluvio-deltaic depositional environments and disrupts the lateral continuity of several sedimentary strata throughout the Park (Dodson, 1971; Wood, 1985, 1989). Such vertical and lateral lithological facies variability

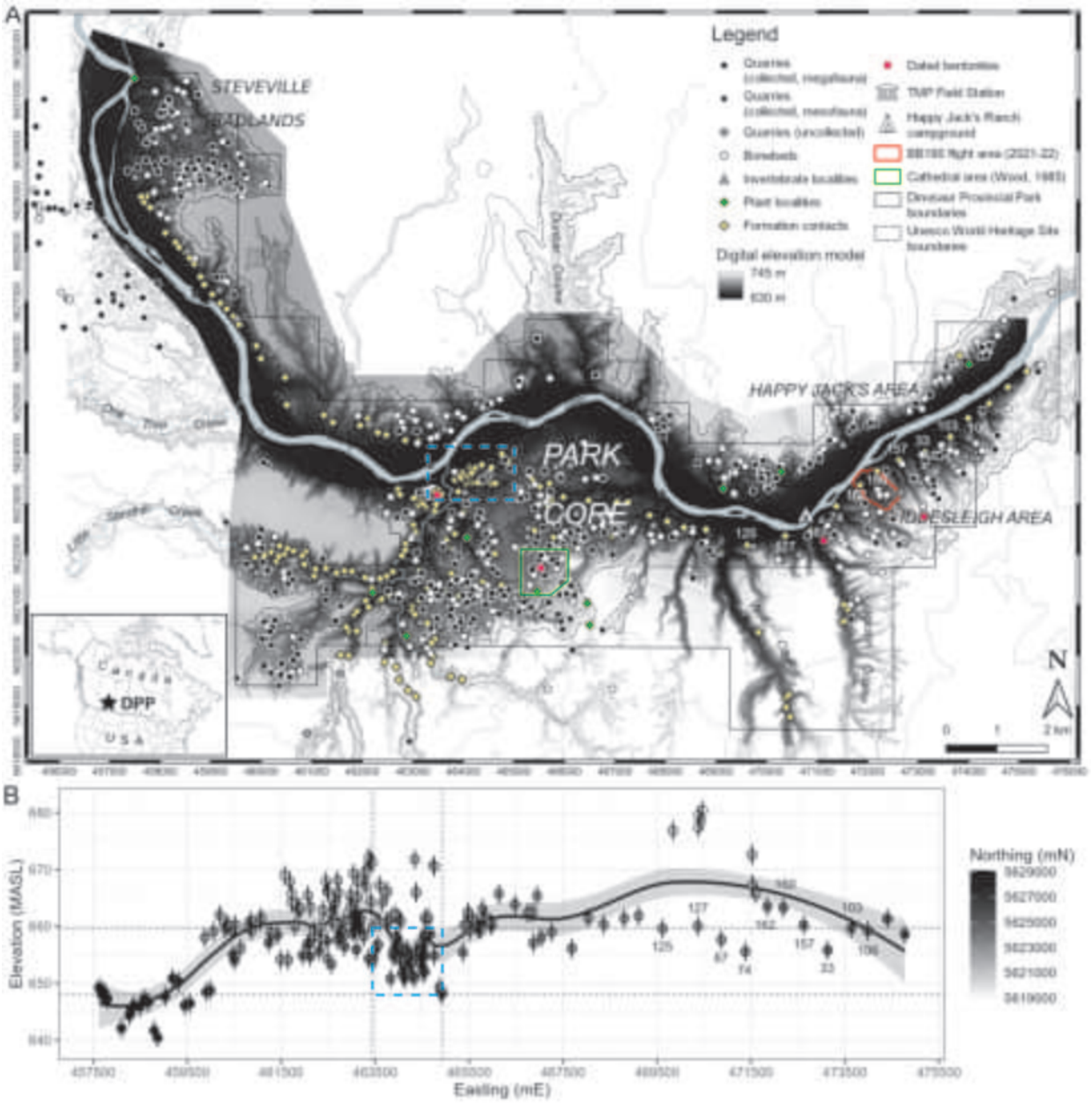

FIGURE 1. Overview of the geological and palaeontological heritage of Dinosaur Provincial Park (DPP) within the context of a digital elevation model (DEM). A, location of drone flight area covering Bonebed 190 among significant fossil quarries and other geological features within DPP. Quarry and formational contact locations available from database assembled by first author, updated from Currie and Koppelhus (2005); bentonite locations available from Ramezani et al. (2022). Numbers indicate Oldman-Dinosaur Park Formation contacts which are compared with OF-DPF contact measured in this study (see Figure 7B). DEM assembled by aerial Lidar scanning in 2015, provided courtesy of Royal Tyrrell Museum of Palaeontology (TMP). Elevation contour lines redrawn from topographic map of DPP (Dinosaur Provincial Park World Heritage Site, 2013) georeferenced on QGIS. B, absolute elevation extracted from TMP DEM for all points measured along OF-DPF contact during a differential GPS survey occurring from 1999 to 2003 along an east-west axis. Coordinates in WGS84 / Universal Transverse Mercator zone 12N, EGM96 geoid. Dashed light blue rectangles indicate same series of points measured around TMP field station and DPP public loop road.

introduces considerable challenges to mapping any outcrop in DPP, let alone sequence stratigraphic correlation attempts. Since mean and maximum offsets between the observed and adjusted stratigraphic positions of specimens above the OF-DPF contact have been estimated at 3.7 and 14.5 m, respectively, quarries located at a similar stratigraphic height in the Park cannot always be assumed to have a similar relative age (Brown, 2013). Ignoring this reality results in a phenomenon known as time-averaging, which is usually defined as the amalgamation of noncontemporaneous fossil remains within a sedimentary unit (Behrensmeyer and Hook, 1992; Behrensmeyer et al., 2000). In localities containing a high density of geographically distinct fossil quarries, such as DPP, those that have a similar stratigraphic height (above the OF-DPF contact) can also be prone to time-averaging since they are not necessarily contemporaneous, thus distorting our perception of biodiversity at any given time interval. The correction of stratigraphic heights of quarries located at the bases of palaeochannel deposits that cut into underlying sediments has been shown to resolve their individual stratigraphic accuracies (Eberth and Getty, 2005; Brown, 2013), although it has limited benefits for a more widespread correlation across the entire Park. Altogether, several assumptions have been made on stratigraphic distributions in the DPP palaeobiota while ignoring potentially crucial stratigraphic and taphonomic limitations on its fossil record's temporal resolution.

Therefore, our motivation for this paper is to determine what is the very highest temporal resolution that could be reached for the Dinosaur Provincial Park palaeobiota while crucially accounting for vertical and horizontal facies variation in the Belly River Group. Specifically, to what extent does the elevation of the OF-DPF contact vary on a very local scale and thus affect the precision the stratigraphic position of DPP's individual fossil quarries? If the OF-DPF contact proves to be an unreliable datum, to what extent can the OF and DPF be subdivided into a series of architectural sedimentary units which could be correlated across long distances? In fact, to what extent would this more resolved chronostratigraphic framework support prevailing biotic turnover hypotheses which are solely founded on biostratigraphy to date? We are now proposing that high-resolution 3-D digital outcrop reconstructions based on aerial surveys of BRG exposures in Dinosaur Provincial Park can provide answers to these questions more efficiently than ground-based surveys alone.

The contribution of aerial surveys to the geology of Dinosaur Provincial Park

Remote sensing methods that combine unmanned aerial vehicle (UAV) flights and structure-from-motion multi-view stereo (SfM-MVS) photogrammetry with ground observations are rapidly evolving in geoscience fields (Colomina and Molina, 2014; Pavlis and Mason, 2017; Nesbit et al., 2020). Image collections acquired in the field can be processed into georeferenced 3-D digital outcrop models (DOMs), 2-D orthomosaics and 2.5-D digital elevation models (DEMs) that provide significant advantages over ground-based large-scale geological surveys, as previously noted (Bond et al., 2007). Most importantly, UAV-based SfM methods reduce or even negate the need for *a posteriori* interpolation between isolated sedimentary logs (i.e., measured stratigraphic sections), which is inevitable in traditional mapping methods and can be error-prone. In a way, their inherent bi- and tridimensionality can be considered to connect one-dimensional dots composed of, for instance, fossil quarry locations and stratigraphic sections on a map. Additionally, their digital outputs have far higher lateral (x, y) and vertical (z) geometrical and locational accuracy than panoramic photographs traditionally used to connect the aforementioned features (see Wood, 1985, 1989; Eberth et al., 2015). UAV-based SfM photogrammetry has already proved highly accurate for the complex badlands landscapes of Dinosaur Provincial Park, where it was applied to decisively support a fully fluvial (as opposed to estuarine or marginal marine) depositional environment for the Dinosaur Park Formation's channel meander belts (Mayo et al., 2023), and to map the migration of one of these sedimentary units (Nesbit et al., 2018; Durkin et al., 2020). A similar method was applied to map the geographic and stratigraphic distributions of fossil remains in the Nemegt Formation of southern Mongolia alongside stratigraphic and taphonomic observations (Fanti et al., 2018, 2024). These studies have shown that lithofacies identifications and measurements obtained from a well-designed DOM are at least as accurate as ground-based measurements, with the aforementioned advantage of lateral facies continuity. Considering these promising findings for the sedimentology of DPP, we have applied UAV-based SfM photogrammetry to identify four vertically successive channel cut-and-fill rhythms over a nearly 500-m^2 area that encompasses the lower half of the Dinosaur Park Formation and surrounds a mixed faunal bonebed (Bonebed 190, see Figure 1A). The identification of

erosional contacts at the base of each of these rhythms also prompted an estimation of the potential surface area of BB190 by tracing the lower contact of its host horizon, as well as an investigation of the effect of local variation in the nearest exposed Oldman-Dinosaur Park Formation (OF-DPF) contact's absolute elevation on the relative heights of the bonebed's main areas of fossil aggregation and of its more isolated individual specimens.

GEOLOGICAL SETTING AND STUDY AREA

The Red Deer River valley within the bounds of Dinosaur Provincial Park displays the largest contiguous badland landscape in Canada, which was formed by bedrock erosion largely triggered by glacial meltwater since the Wisconsinian deglaciation ~15 k.y.a. during the retreat of the Laurentide ice cap (Campbell, 1970; Evans, 2000). The dominance of smectite-rich sandstones, siltstones and mudstones in these outcrops combined with a seasonally semi-arid regional climate with intense wind, rainfall and fluvial runoff episodes contribute to high erosion rates of 4 mm/year on average (Campbell, 1970; Eberth, 2005). This erosion has produced a constantly changing mosaic of buttes, mesas, rills, coulees and hoodoos with very sparse vegetation between river and prairie levels, thus presenting ideal conditions for exposing fossils. The badlands of DPP record the upper ~100 m of the 280 m thick Belly River Group. The uppermost 10-20 m of the Oldman Formation (OF) are exposed, overlain disconformably by the ~80 m thick Dinosaur Park Formation (DPF), which is itself gradationally overlain by marine shales of the Bearpaw Formation (Eberth and Hamblin, 1993; Eberth, 2005; Eberth et al., 2023). Those bedrock exposures are broadly stacked horizontally, with a ~0.05º dip to the northwest characteristic of all Upper Cretaceous strata in the North American Great Plains (Dawson et al., 1994; Eberth, 2005; Nesbit et al., 2018). Although the OF originated from a lobe of the Judith River-Belly River clastic wedge that deposited sediments in a general northeasterly direction during the Claggett marine regressive cycle, the DPF originated from a separate clastic lobe that deposited sediments in a general southeast direction into a subsiding foreland basin that was undergoing increased accommodation and sediment supply throughout the Bearpaw transgressive cycle (Cant and Stockmal, 1989; Eberth and Hamblin, 1993; Hamblin, 1997). These formations thus represent distinct events in the broader depositional history of the Belly River Group's clastic wedge, which has been shown to be more influenced by the North American Cordillera's tectonic activity (on a regional scale) than by the eustatic sea level rise which was occurring on a global scale throughout the latest Campanian (Cant and Stockmal, 1989; Eberth et al., 2023). The contact between the sedimentary packages deposited by these two clastic lobes in DPP represents a hiatus between their respective times of deposition, and forms an erosional discontinuity which is consistently identifiable by (1) a marked facies transition from the pale ochre iron-stained sandstones of the OF to a mosaic of pale gray (often trough cross-bedded) sandstones characteristic of the DPF, and (2) contrasting gamma-ray signatures from subsurface well logs throughout southern Alberta (Eberth and Hamblin, 1993; Eberth, 2005, 2024; Eberth et al., 2023). The latest U-Pb zircon ages reveal that the OF-DPF contact forms an isochronous datum in DPP and in north-central Montana dated at ca. 76.3 m.y.a. (Rogers et al., 2023), although it still appears to be time-transgressive throughout southernmost Alberta and southwestern Saskatchewan (Eberth and Hamblin, 1993; Chiba et al., 2015; Evans, et al., 2015; Eberth, 2024). Despite this growing chronostratigraphic significance across the Western Interior Basin, the OF-DPF contact's absolute elevation has been shown to vary by up to ~30 m on a regional scale (i.e., over several kilometres) across the entire breadth of DPP (Eberth and Hamblin, 1993; Eberth, 2005; Figure 1B). Such a trend now raises the possibility that the elevation of this same contact could vary as substantially on a more local scale (i.e., over horizontal distances of a few hundred metres) within the present study area around Bonebed 190.

The sedimentary layers of the Dinosaur Park Formation are interpreted as successive channel meander belts cutting into (then migrating along) a wide floodplain that stretched along the eastern shore of Laramidia, with an average palaeocurrent flowing east-southeast into the advancing Bearpaw Sea (Koster et al., 1987; Wood et al., 1988; Wood, 1989; Hamblin, 1997). Channel cut-and-fill cycles can be designated as 'rhythms' *sensu* Wood (1985) and consist of fining-upward sequences composed of at least two of the four major lithofacies of the DPF. In order of grain size from the coarsest (indicating a high-energy depositional setting) to the finest (low-energy), these lithofacies are (1) trough cross-bedded sandstones (TX) interpreted as either channel lag or lower point bar deposits; (2) inclined bedding sandstones (IBS)

interpreted as mid-to-upper point bar lateral accretion deposits; (3) inclined heterolithic strata (IHS) consisting of interbedded sandstone and siltstone with varying ratios, interpreted as mid-to-upper point bar lateral accretion deposits with fluctuating hydraulic energy (Koster, 1983; Thomas et al., 1987); and (4) siltstones and mudstones interpreted as overbank (i.e., abandoned channel fill) deposits. The most ambitious detailed stratigraphy ever achieved in DPP has been undertaken over ~1 km^2 in the Cathedral area in the Park's Core (Wood, 1985; Figure 1A): it led to the identification of six channel cut-and-fill rhythms constrained by erosional contacts, which were recognized by the presence of channel lags containing intraclasts, clay-ironstone pebbles and organic debris (including fossils). Any erosional contact is thus considered a more robust datum between different channel cut-and-fill cycles than a gradational contact between TX and IHS or TX and IBS that only reflects the lateral accretion of point bars formed by the same channel (Wood, 1989). Furthermore, sandstone ribbons less than 10 cm thick (interpreted as ephemeral channels pinching out at their lateral extremities) were distinguished from deeper and more laterally continuous sandstone members. Overall, these initial studies of the alluvial architecture of the DPF exposed in DPP have laid the groundwork for a correlation of individual fossil localities at a greater spatial scale. The sedimentological principles they established have now been applied to identify equivalent architectural units in a different region of the Park with a similar order of magnitude in surface area, in this case as a means to achieve chronostratigraphic research objectives with palaeoecological implications.

Bonebed 190 is located in the Iddesleigh area of Dinosaur Provincial Park, which includes approximately the eastern third of the Red Deer River's right bank within the Park's boundaries (Figure 1A). Although this region has been historically less explored than the Core or the Steveville badlands due to its relative isolation, it has still produced unique and spectacular vertebrate specimens, such as the near-complete holotypes of the centrosaurine ceratopsid *Styracosaurus albertensis* (Quarry 16) and the ankylosaurid *Scolosaurus cutleri* (Q080) (Lambe, 1913; Nopcsa, 1928) as well as an unnamed pachyrhinosaur similar to *Achelousaurus* recovered much more recently from the Lethbridge Coal Zone (Q240) (Ryan et al., 2010). It also contains a dense *Centrosaurus apertus*-dominated bonebed (BB180) whose exploration led to the Park's most recently discovered bentonite, which provided additional radioisotopic dates for the local Belly River Group (Brown et al., 2020; Ramezani et al., 2022; Eberth et al., 2023). BB190 itself is located near the summit of a plateau that includes the upper Oldman Formation and the lower half (~40 m) of the Dinosaur Park Formation. It was first discovered on July 19, 2002, during fieldwork led by Mike Archer and Henk Godthelp (Australian Museum) (Currie, personal commun., 2022) and classified as a multigeneric (mixed faunal) bonebed due to its considerable vertebrate macro- and microfossil diversity (see Eberth and Currie, 2005). One of the most significant specimens of the initial BB190 collection consists of centrosaurine partial parietals (TMP2005.009.0069) that cannot be identified at a lower taxonomic level due to their lack of preserved diagnostic characters, although they appear more similar to *C. apertus* than to *Styracosaurus albertensis* (Royal Tyrrell Collections, 2023). Considering that these two species seem to be key members of successive megaherbivore assemblage zones in the DPF (Ryan and Evans, 2005; Mallon et al., 2012), the high apparent stratigraphic proximity of BB190 to the hypothetical boundary between these two biozones deserved further attention.

BB190 was not explored again until June 2018, when a crew of McGill University's Vertebrate Palaeontology field course found new potential outcrops of that locality in collaboration with the University of Alberta. The combination of high observed diversity with high preservation quality in BB190 initiated a long-term project aiming to estimate that bonebed's species richness and taxon abundances. Furthermore, an extensive Oldman-Dinosaur Park Formation contact was identified along a wide coulee (i.e., a canyon typical of badlands landscapes). This coulee is located far closer to BB190 than the nearest previously identified contacts (marked as Contacts 160 and 162, see Currie and Koppelhus, 2005). This discovery therefore laid an additional foundation for the following study of the bonebed's geological setting since it provided an opportunity to quantify uncertainties in the stratigraphic position of BB190 while simultaneously identifying architectural units with potential stratigraphic relevance that extend beyond the study area.

MATERIAL AND METHODS

The methods outlined in this paper consist of three main steps: (1) raw data acquisition in the field (i.e., aerial images and GPS coordinates); (2)

georeferenced reconstruction of the study area through photogrammetry; (3) geospatial data analysis (i.e., lithofacies identification and horizontal and vertical distance measurements). Additional information on each of these steps is provided in Appendix 1.

Fieldwork – aerial and ground-based data acquisition

The first two UAV flights conducted around BB190 occurred in 2021 and together covered the entire extent of the mapped area (~0.5 km^2). A third flight occurred in 2022 and covered a more restricted area around the most continuous exposure of the Oldman-Dinosaur Park Formation contact near the bonebed. Two multirotor UAVs were selected: a DJI Mavic 2 Pro with a 16.8 megapixel (MP) digital camera, and a smaller DJI Mavic Air2S with a 20 MP camera. For the 2021 flights, the DJI Mavic 2 Pro covered the entire mapped area ~80 m above ground level in generally parallel flight lines, capturing 669 images at a 0˚ pitch angle off-nadir over ~30 minutes, while the DJI Mavic Air2S was flown solely over the sandstone horizon hosting BB190 ~50 m above ground level along a relatively free flight path, capturing 99 images at a 0˚ pitch angle over ~15 minutes (Figure 2A-D). The 2022 flights only involved the DJI Mavic 2 Pro, with the first 285 images captured ~50 m above the top of the escarpment bearing the most clearly exposed OF-DPF contact at a 0˚ pitch angle over ~15 minutes, followed by 67 images captured at a ~20 m lower elevation with a 45˚ camera pitch angle over ~5 minutes to enhance coverage of the contact's subvertical surface (Figure 2C). A total of 1,120 images were thus recorded and processed from these flights.

Ground control points (GCPs) were marked and measured with a SXBlue II + GNSS receiver (Geneq. Inc., Montréal, Québec, Canada) for each flight day (Table 1; Figure 2E-F) to increase the geolocation accuracy of reconstructions arising from these aerial surveys. Around one hour (excluding UAV flight time) was spent laying, marking, and subsequently removing GCPs across the flight areas during each of the two flight days. No attempt was made to increase GCP positional accuracy through real-time kinematics (RTK) or post-processing kinematics (PPK) in this study, although we have started applying these techniques as part of a broader mapping project for DPP (see Discussion). Fossil specimen coordinates and stratigraphic measurements were also acquired from ground-based surveys of the BB190 area (Table 2). As the lateral extent of BB190 was expanded, some of these specimen locations became reference points for newly identified outcrops of the bonebed, which were assigned quarry numbers BB190A-C. Stratigraphic sections were also measured on foot during the 2022 field season to establish the bonebed's geological setting with a more traditional method, using Jacob's staffs and Brunton compasses to establish bedding thicknesses. The most extensive section was measured along a footpath leading to the bonebed's northwest corner, and a much more constrained section was measured immediately above and below an overbank deposit marked as BB303 due to its higher stratigraphic position compared with other outcrops of the bonebed (Figure 2E).

UAV data processing

The UAV images were processed through structure-from-motion photogrammetry (SfM), an emerging 3-D modeling method based on overlapping 2-D images captured from a device in motion (see Nesbit et al., 2018 and references therein). SfM was performed using Agisoft Metashape Professional version 2.0.2, build 16404 (commercial software, Agisoft LLC, St. Petersburg, Russia), and a high-performance workstation (Intel® Core™ i7-7820X central processing unit (CPU) at 3.60 GHz with 127.68 GB of random-access memory (RAM) and a NVIDIA GeForce GTX 1080 Ti graphics card). The SfM photogrammetry workflow was applied through the following steps. First, all images were imported into the same Agisoft project and aligned at the highest possible accuracy through detection of automatic tie points shared by overlapping images (Figure 2A-D). Image alignment resulted in a dense 3-D point cloud georeferenced using a combination of the geotags from the UAVs' GPS receivers and the GPS readings obtained in the field for GCPs. The dense point cloud was converted in two parallel workflows: (1) a 2.5-D digital elevation model (DEM, see Figure 2E) leading to a 2-D orthomosaic and (2) an interpolated 3-D mesh. Additional details about SfM photogrammetry are available as an Agisoft processing report in Appendix 2.

Geospatial data analysis

2-D, 2.5-D and 3-D data visualization. The DEM and orthomosaic were exported from Agisoft and imported into QGIS 3.24.1 'Tisler', to visually represent possible contacts between sedimentary architectural units and to quantify their elevation variation. These files were imported alongside the

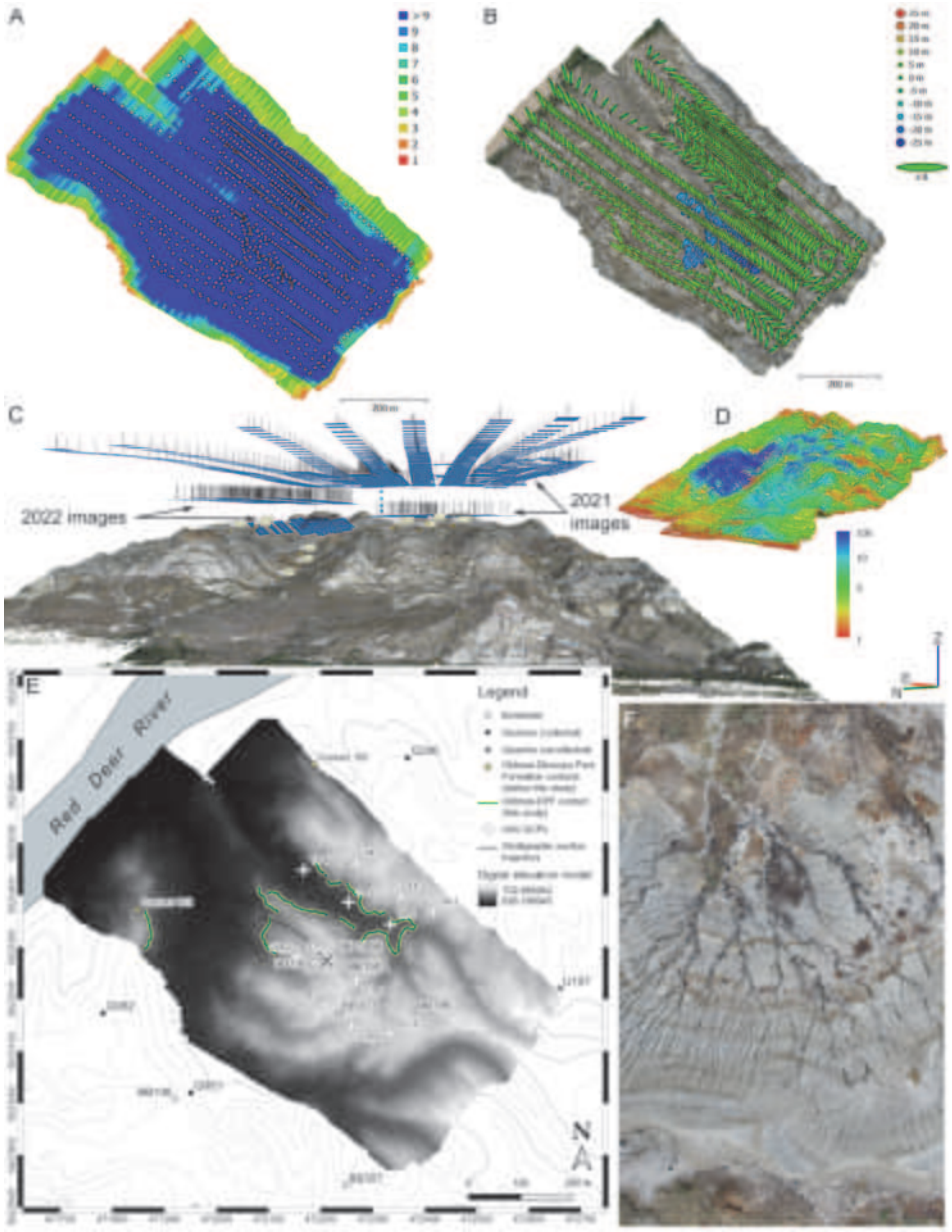

FIGURE 2. Overview of unmanned aerial vehicle (UAV) structure-from-motion (SfM) photogrammetry process leading to creation of digital outcrop model (DOM), digital elevation model (DEM) and orthomosaic of Bonebed 190 Amphitheatre area; survey area 0.446 km^2. A, UAV camera locations and image overlap obtained from Agisoft Metashape processing report: colour palette indicates number of overlapping images per grid cell. B, UAV camera location error estimates along flight paths obtained from Agisoft Metashape processing report: Z error represented by ellipse colour; X, Y errors represented by ellipse shape; estimated camera locations marked with black dot. C, perspective render of dense 3-D point cloud generated from UAV image alignment followed by geolocation optimization with ground control points (GCPs, marked with flags). Image dataset combined from 2021 and 2022 flights; 2022 images (including some taken at 45˚ pitch angle) cover well-exposed Oldman-Dinosaur Park Formation contact. D, orthographic render of dense 3-D point cloud coloured by point confidence; blue represents highest point confidence, as seen on the outcrop photographed at oblique angles (see Figure 2C). E, DEM with GCP locations, significant fossil quarries and measured Oldman-Dinosaur Park Formation contacts. Coordinates in WGS84 / Universal Transverse Mercator zone 12N, EGM96 geoid. Quarry and formational contact locations available from database assembled by first author, updated from Currie and Koppelhus (2005). Black crosses mark start and end points of main stratigraphic section measured during 2022 field season. F, inset of image captured during 2021 flight at low elevation over BB190 host horizon; note GCP made of two white Jacob's staffs (GCP 21_3 in Figure 2E).

TABLE 1. Ground control point measurements for Bonebed 190 Amphitheatre area mapping project. All coordinates in WGS84 horizontal datum, EGM96 geoid. X, Y, and Z errors refer to positional accuracy of SXBlue II + GNSS receiver used in the field.

Date	GCP No.	Latitude	Longitude	Elevation (m)	X/Y error (m)	Z error (m)
2021-08-21	21-1	50.76065238	-111.3940977	688.68	0.6	1.2
2021-08-21	21-2	50.7606319	-111.3947881	688.38	0.6	1.2
2021-08-21	21-3	50.75978285	-111.3940391	689.56	0.6	1.2
2021-08-21	21-4	50.75942865	-111.3933062	686.38	0.6	1.2
2021-08-21	21-5	50.75931225	-111.39224	687.28	0.6	1.2
2021-08-21	21-6	50.76023237	-111.3931835	688.35	0.6	1.2
2022-08-14	14-1	50.761436	-111.391109	688.0	0.586	1.171
2022-08-14	14-2	50.761691	-111.391974	687.2	0.491	0.981
2022-08-14	14-3	50.762264	-111.393195	689.753	0.502	1.003
2022-08-14	14-4	50.762137	-111.394635	643.533	0.512	1.024
2022-08-14	14-5	50.761586	-111.39341	646.526	0.543	1.085
2022-08-14	14-6	50.761201	-111.392262	652.601	0.632	1.264

coordinates of fossil specimens collected from BB190 during this study, as well as all fossil and formational contact locality coordinates previously known from DPP (updated from Currie and Koppelhus, 2005). Furthermore, a DEM of the entire Park curated at (and obtained from) the Royal Tyrrell Museum of Palaeontology (TMP) was imported into the same QGIS project (see Figure 1) to compare elevation measurements within the mapped BB190 area with other DPP localities.

Digital lithofacies identification. The succession of sedimentary facies was carefully examined on the orthomosaic, complemented by surveys of the DOM in Agisoft. The resolution of the DOM and orthomosaic texture enabled the identification of three main facies, which broadly correspond to the 'digital facies' (dF) of Nesbit et al. (2018). Coarse-grained facies were identified as sandstone (dF1), which include massive, cross-bedded and ripple-laminated sandstones. Facies displaying interbedded sandstones and siltstones were identified as inclined heterolithic strata (IHS, corresponding to dF2 and dF3). Thick fine-grained facies were digitally identified as mudstones (broadly corresponding to dF4). Facies identification enabled tracing polylines along continuous contacts identified between architectural units, as well as correcting the identity of some lithological units which were erroneously identified in the ground-based stratigraphic section. Elevation contour lines were extracted in QGIS from the BB190 DEM (one dataset at 5 m intervals and another at 1 m intervals) and saved in a layer overlying the orthomosaic surface to rapidly assess elevation variation within and among neighbouring contacts during the polyline tracing process.

Horizontal and vertical distance measurements. The horizontal length of each of the lower contacts of rhythms identified around BB190 was measured as the sum of the distances calculated for each polyline traced along the orthomosaic in QGIS. This is also where the bonebed's minimum surface area was calculated by connecting its most distant fossil localities with a polygon. The GPS readings recorded for the most significant collected fossils enabled comparisons of absolute and relative elevations between field-based and DEM-derived estimates. For each of the continuous contacts exposed throughout the BB190 mapped area, series of points were produced from their corresponding polylines at a 5 m interval for graphical and statistical analyses on elevations of fossils and architectural unit contacts in R v 2024.04.0 build 735 (R Core Team, 2023). The data and code for these analyses are available as Appendices 3-7.

The elevation of the Oldman-Dinosaur Park Formation (OF-DPF) contact identified around BB190 was compared with those of 10 previously identified contacts located east and west of that locality along the Red Deer River's right bank (in the Iddesleigh area of the Park). This necessitated extracting coordinates from the DEM covering the entire Park (beyond the immediate BB190 area). With this data, the variability in the elevation of the OF-DPF contact could be compared between a region where that contact was measured repeatedly at a very high spatial density (within the BB190 mapped area) and a more extensive region

TABLE 2. Coordinates for BB190 fossil specimens, quarry stakes and nearby formational contacts. Coordinates recorded with WGS84 / UTM zone 12N projected coordinate system, except if recorded with SXBlue II + GNSS receiver (originally in decimal degrees then transformed to facilitate comparisons here); vertical coordinates using EGM96 geoid. Ortho relocation means that specimen location was never recorded with GPS, instead its quarry was relocated on the orthomosaic. **Abbreviations: DEM,** digital elevation model; **DGPS,** differential GPS receiver; **MASL,** metres above sea level; **OF-DPF,** Oldman-Dinosaur Park Formation contact; **SD,** standard deviation. All relative elevations (heights) calculated from Z coordinates extracted from DEM generated for this study; features marked in bold used as check points to measure root mean square error of BB190 DEM generated for this study.

Feature	Locality	Measurement year; method	Easting (mE)	Northing (mN)	GPS elev. ± Z error (MASL)	BB190 DEM elev ± 1.09 (MASL)	Mean height Contacts 160;162 ± SD 1.89 (m)	Mean height 10 nearby OF-DPF contacts ± SD 1.94 (m)	Mean height 11 distant OF-DPF contacts ± SD 2.95 (m)	Height Rhythm 4 ± 2.18 (m)
BB190	BB190 (Original)	2002; DGPS	472379	5623176	687.7 ± 0.1	686.6	24.32	26.92	26.85	NA
BB190A stake	BB190A	2018; Garmin	472246	5623249	689 ± 5	687.7	25.45	28.06	27.99	0.16
Ceratopsid pubis	BB190B (stake)	2023; Garmin	472232	5623289	687 ± 3	688.0	25.77	28.37	28.30	0.50
Centrosaurine nasal horn core	BB190C (stake)	2022; SX Blue	472197	5623282	688.2 ± 1.1	688.8	26.58	29.18	29.11	0.44
Hadrosaurid maxilla	BB303 (stake)	2022; SX Blue	472236	5623173	688 ± 0.6	687.9	25.67	28.27	28.20	0.85
Microsite 2018	BB190 (Original)	2018; Garmin	472389	5623173	684 ± 5	685.9	23.67	26.27	26.20	0.66
Microsite 2019	BB190 (Original)	2019; Garmin	472378	5623183	684 ± 5	685.8	23.51	26.11	26.05	-0.01
Quarry A NW stake	BB190A	2023; ortho	472237.85	5623253.05	NA	687.9	25.65	28.25	28.18	NA
Quarry A SE stake	BB190A	2023; ortho	472247.7	5623247.5	NA	687.6	25.35	27.95	27.88	NA
Quarry B NW stake	BB190B	2021; Garmin	472221.8	5623296.8	682.25 ± 5	688.8	26.55	29.15	29.08	NA
Quarry B SE stake	BB190B	2021; Garmin	472227	5623293.2	NA	688.7	26.45	29.05	28.98	NA
Centrosaurine squamosal	BB190 (other)	2018; Garmin	472160	5623186	685 ± 5	688.4	26.15	28.75	28.68	1.45
Ceratopsid ilium	BB190A	2021; Garmin	472242.89	5623241.03	681.64 ± 5	688.2	25.92	28.52	28.45	0.76
Ceratopsid skull element	BB190C	2019; Garmin	472202	5623283	690 ± 5	688.6	26.33	28.93	28.86	0.39
Hadrosaurid humerus	BB303	2022; ortho; Garmin	472239	5623173	NA	688.2	25.97	28.57	28.50	1.15
Hadrosaurid maxilla fragment	BB190 (other)	2023; Garmin	472500	5623158	695 ± 4	692.1	29.82	32.43	32.36	9.94
Hadrosaurid braincase	BB303	2022; SX Blue	472242	5623171	688 ± 0.8	688.5	26.25	28.85	28.79	1.43
Hadrosaurid left dentary	BB190 (other)	2023; Garmin	472432	5623210	695 ± 3	691.7	29.43	32.03	31.96	8.24
Hadrosaurid sternal plate	BB190 (other)	2018; Garmin	472201	5623182	685 ± 5	690.0	27.78	30.38	30.31	1.31
Hadrosaurid femur	BB190 (other)	2019; ortho; Garmin	472207.8	5623186.9	NA	688.7	26.49	29.09	29.02	0.72

TABLE 2 (continued).

Feature	Locality	Measurement year; method	Easting (mE)	Northing (mN)	GPS elev. ± Z error (MASL)	BB190 DEM elev ± 1.09 (MASL)	Mean height Contacts 160;162 ± SD 1.89 (m)	Mean height 10 nearby OF-DPF contacts ± SD 1.94 (m)	Mean height 11 distant OF-DPF contacts ± SD 2.95 (m)	Height Rhythm 4 ± 2.18 (m)
Hadrosaurid tibia	BB190A	2022; Garmin	472283	5623249	686 ± 5	688.1	25.84	28.44	28.37	0.34
Subadult hadrosaurid tibia	BB190 (other)	2019; Garmin	472336	5623133	686 ± 5	687.2	24.97	27.57	27.50	2.35
Hadrosaurid foot bones	BB190B	2021; Garmin	472226.2	5623283.5	688.12 ± 5	689.3	27.04	29.64	29.57	1.77
Hadrosaurid metatarsal	BB190C	2022; SX Blue	472199	5623268	689 ± 1.2	689.7	27.40	30.01	29.94	1.32
Juvenile hadrosaurid dentary	BB190 (other)	2018; Garmin	472270	5623152	685 ± 5	687.6	25.37	27.97	27.90	1.52
Ornithomimid ischium	BB190C	2019; Garmin	472203	5623287	690 ± 5	689.0	25.84	28.44	28.37	-0.10
Ornithomimid humerus	BB190B	2022; Garmin	472229	5623295	685 ± 5	688.3	26.01	28.61	28.54	0.63
Tyrannosaurid nasals	BB190 (other)	2023; Garmin	472288	5623182	688 ± 3	689.9	27.62	30.22	30.15	1.62
Tyrannosaurid dentary	BB190 (Original)	2022; ortho	472372.4	5623193.5	NA	686.5	24.25	26.85	26.78	0.06
Troodontid metatarsal	BB190A	2022; SX Blue	472270	5623237	686 ± 0.8	687.6	25.33	27.93	27.86	0.36
Theropod tarsal element	BB190 (other)	2023; Garmin	472231	5623160	691 ± 2	688.5	26.31	28.90	28.83	0.83
Ornithischian long bone fragment (not collected)	BB190 (other)	2018; Garmin	472253	5623230	NA	689.9	27.64	30.24	30.17	NA
Contact 160	NA	1999-2003; DGPS	472186.859	5623651.467	663. ± 0.1	660.9	NA	NA	NA	NA
Contact 162	NA	1999-2003; DGPS	471847.626	5623372.669	663.2 ± 0.1	663.6	NA	NA	NA	NA

where it was measured at a much lower density (i.e., previously identified contact locations). The mean elevation of the contact points sampled around BB190 was also compared with that of 48 contact locations along the Park's public loop road (see Figure 1B), since the latter is the area of the Park where the OF-DPF contact was measured at the highest frequency prior to this study. Additionally, mean heights and standard deviations above the OF-DPF contact for the main quarries identified across BB190 (obtained from the DEM generated in this study) were compared between three groups of selected contacts: (1) Contacts 160 and 162; (2) 10 contacts sampled within a very localized area, at 15-20 m intervals along the north slope of the coulee with the most continuous OF-DPF contact exposures; (3) 11 contacts sampled across the entire extent of the BB190 DEM (including Contacts 160 and 162). To quantify the elevation uncertainties of the DEMs used in this study, their respective root mean square errors (RMSE) were calculated using fossil quarries with available GPS readings as check points (see Appendix 1 for more details).

RESULTS

The mapping project of the outcrops surrounding BB190 produced through SfM photogrammetry covered 0.446 km^2 of Dinosaur

FIGURE 3. Orthomosaic of Bonebed 190 Amphitheatre area highlighting contacts between identified architectural sedimentary units. Coordinates in WGS84 / Universal Transverse Mercator zone 12N. 'BB190' point marks original quarry stake marked in 2002; 'BB190A-C' and 'BB303' points mark fossil-rich localities discovered during this study. Note semi-circular shape formed by ridge marked by dark red contact between Rhythm 3 mudstone and Rhythm 4, hence the proposed 'Amphitheatre' toponym. Quarry and formational contact locations available from database assembled by first author, updated from Currie and Koppelhus (2005).

Provincial Park, at a ground resolution of 1.91 cm/pixel, with a GCP elevation RMSE of ±0.42 m and a DEM elevation RMSE of ±1.09 m. A summary examination of the orthomosaic reveals that BB190 is located at the summit of a plateau that widens between two primary coulees flowing to the northwest (Figure 3). The plateau displays crenellated northern and western margins created by alternating rills and coulees. The bonebed's host horizon is a thick sandstone preserved in a nearly semi-circular shape with lower horizons dipping towards the circle's centroid, hence the designation of this entire plateau as the BB190 Amphitheatre area. Almost all the fossils found within the orthomosaic's extent during this study have been uncovered along the lower contact of this sandstone unit. The minimal surface area of BB190 has been estimated at ~91,200 m^2 by connecting its most distant confirmed fossil localities into a polygon on QGIS. A 4.5-minute video of a virtual tour of the digital outcrop model is available as Appendix 8.

Description of architectural units

The Dinosaur Park Formation in the BB190 Amphitheatre area is interpreted to contain a succession of four channel cut-and-fill rhythms through time above the Oldman Formation. They were identified by examining the entire extent of the DOM and orthomosaic and were all found at the site of the main stratigraphic section as well (Figure 4A-B).

The Oldman-Dinosaur Park Formation contact. The coulee that forms the northern margin of the BB190 Amphitheatre area has the longest continuous outcrops of the Oldman-Dinosaur Park Formation (OF-DPF) contact in the study area (Figure 3). These exposures lie further away from the river than the two contact points that were previously measured in the vicinity (Contacts 160, 162). They display a sedimentary transition which is always indicative of the presence of this formational contact, from the massive ochre coarse-grained sandstones of the Oldman Formation to the pale grey, often trough cross-bedded, sandstones of the Dinosaur Park Formation (Figure 5A-C). The OF-DPF contact is also detected, albeit less extensively, in a secondary coulee along which the stratigraphic section was measured (Figures 4A-B, 6A), as well as a butte located west of the BB190 Amphitheatre area along which Contact 162 was measured. The ochre to grey sandstone succession is often broken by a massive silty ironstone whose upper margin is level with the contact (Figure 5A-B). This facies is common across the Park at this level (Eberth et al., 2023, figure 2), although it is locally replaced by a clay-ironstone intraclast table in the coulee where the stratigraphic section was measured (elevation of 658 ±1 m, Figure 4A-B).

The OF-DPF contact had variable elevations that were quantified across the BB190 mapped area (Figure 7A-B). Across both northern and southern slopes of the aforementioned coulee, the contact's absolute elevation fluctuated significantly since the root mean square error (RMSE) of 1.09 m derived from the DEM is far lower than the observed elevation range of 8.36 ± 2.18 m (Table 3; Figure 7A). The northern slope's contact (shown on Figure 5A-B) has a mean height of 659.79 m with a standard deviation of 1.52 m. That same contact was selected to sample points as references for the relative height of BB190 quarries and fossils. The southern slope's contact has a mean height of 660.38 m with a standard deviation of 2.22 m. The elevation range of all 182 OF-DPF contacts within the BB190 mapped area (including less extensive contact exposures) was then compared to that of the 10 nearest contact localities known prior to this study, distributed along the entire eastern third of the Red Deer River's right bank within DPP (Figures 1A-B, 7B). In this dataset (based on the DEM covering the entire Park), the BB190 contact series is shown to have an elevation range of 11.52 ± 3.44 m and a mean elevation of 658.64 m with a standard deviation of 2.47 m (Table 3). The 10 other contacts have an elevation range of 7.92 ± 3.44 m, with a mean elevation of 659.46 m and a standard deviation of 2.66 m. The high density of points sampled from the BB190 contact series also reveals frequent fluctuations in absolute elevation, with at least 3 apparent peaks over an east-west transect of barely 600 m. That local variability is higher than in the 10 other contact points (likely due to a higher sample size covering a smaller geographical area), yet a Wilcoxon rank-sum test revealed that the means between the two groups do not differ significantly (W = 743, *p*-value = 0.3305, see Appendices 1 and 3). Considering the small size of the latter sample, the BB190 OF-DPF contact was then compared with one of the OF-DPF contact exposures with the highest density of measured points prior to this study, the ~2 km^2 area that includes the Royal Tyrrell Museum field station and the Park's public loop road (Figure 1A-B). Those 48 sampled points have an elevation range of 11.51 ± 3.44 m, with a mean elevation of 654.28 m and a standard deviation of 2.88 m (Table 3). A Wilcoxon rank-sum test was performed between the 'public loop road' and BB190 groups and showed that the contact around the public loop road has a significantly lower mean elevation than the contact in the BB190 Amphitheatre area (W = 7639, *p*-value = $1.52e^{-15}$). The Oldman Formation is exposed for 12-15 m depths below the OF-DPF contact in the BB190 Amphitheatre area, which is consistent with analogous outcrops throughout the Park.

Rhythm 1. The OF-DPF contact is considered a reliable datum for the base of Rhythm 1. It is confidently identified for 821 of the 1,595 m traced on the entire orthomosaic for Rhythm 1's lower contact and tentatively identified for the remaining distance. The only feature indicative of the contact for the remainder of that distance is the massive silty ironstone cap that often crops out at this level (Figure 4A). The depth of Rhythm 1 varies between 5.6 and 11.5 m across the 11 digital sections along which it was measured (Table 4). This variation is attributed to exposures where its channel base dips significantly (see Figure 5C) combined with

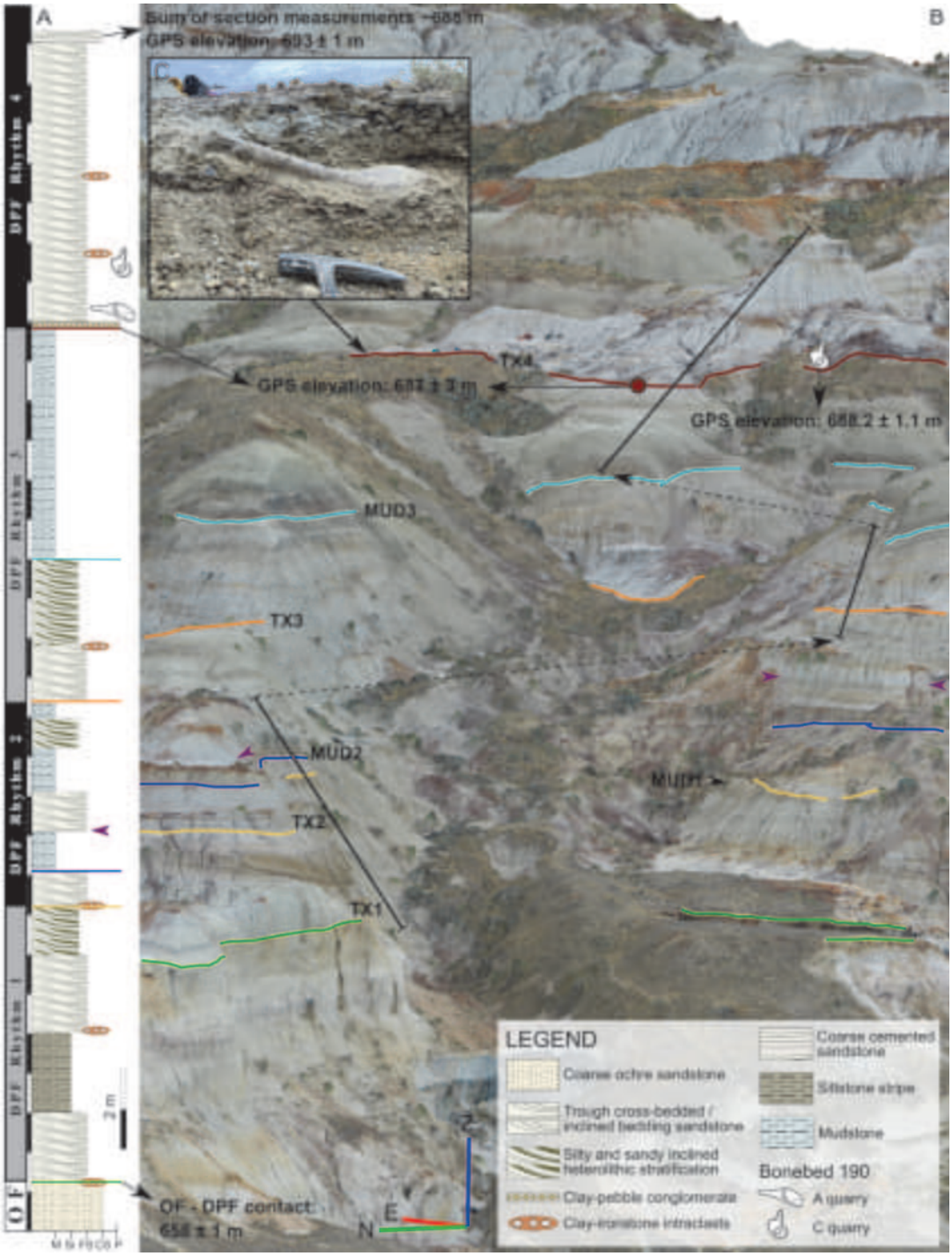

FIGURE 4. Visualization of architectural units of BB190 Amphitheatre area using stratigraphic section and digital outcrop model (DOM). A, stratigraphic section measured along secondary coulee leading to BB190. B, orthographic render of DOM displaying outcrop exposures measured for stratigraphic section. C, cross-sectional photograph of clay-pebble conglomerate forming erosional contact between MUD3 and TX4, hosting ceratopsid pubis collected from BB190B quarry. Colour code for lower contacts of architectural sedimentary units identified across entire mapped area same as in Figure 3; burgundy arrowheads mark sandstone ribbon cutting into MUD2. Black strokes indicate extent of measured outcrops, dashed arrows indicate interruptions in continuous sequence measurements. Lower half of section corrected during examination of DOM after fieldwork. **Abbreviations: M** and **MUD,** mudstone; **Si,** siltstone; **FS,** fine-grained sandstone; **CS,** coarse-grained sandstone; **P,** pebbles; **TX,** trough cross-bedded sandstone; **DPF,** Dinosaur Park Formation; **OF,** Oldman Formation.

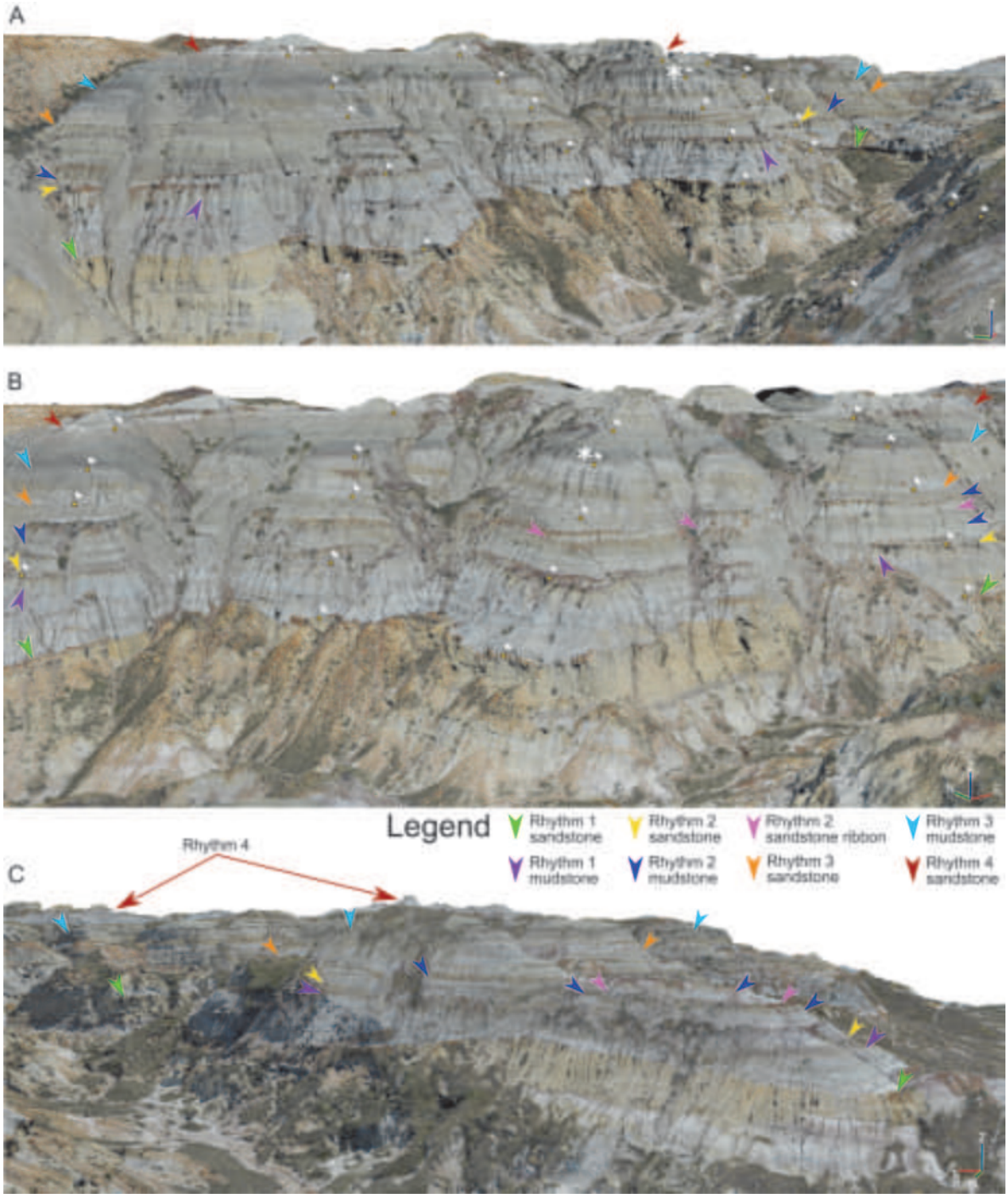

FIGURE 5. Perspective renders of digital outcrop model (DOM) highlighting channel cut-and-fill rhythm succession above a continuously exposed Oldman-Dinosaur Park Formation (OF-DPF) contact extending along both flanks of the coulee located along the northern margin of the BB190 Amphitheatre area. OF-DPF contact marks base of Rhythm 1 sandstone. A, exposure on northern slope of the coulee. B, close-up of A from a different viewing angle; note occasional thick blocks of silty ironstone at the OF-DPF contact, dark red clay-ironstone table at base of Rhythm 2 sandstone and laterally discontinuous sandstone ribbon cutting within Rhythm 2 mudstone. C, exposure on southern flank of the coulee; note southeastward slump in OF-DPF contact and vertical amalgamation of sandstone units pinching out mudstone units to the southeast. Ticks mark bases of each identified lithological unit, points marked with flags indicate digital sections traced to measure local rhythm depths in Agisoft, white asterisk indicates same location in A and B.

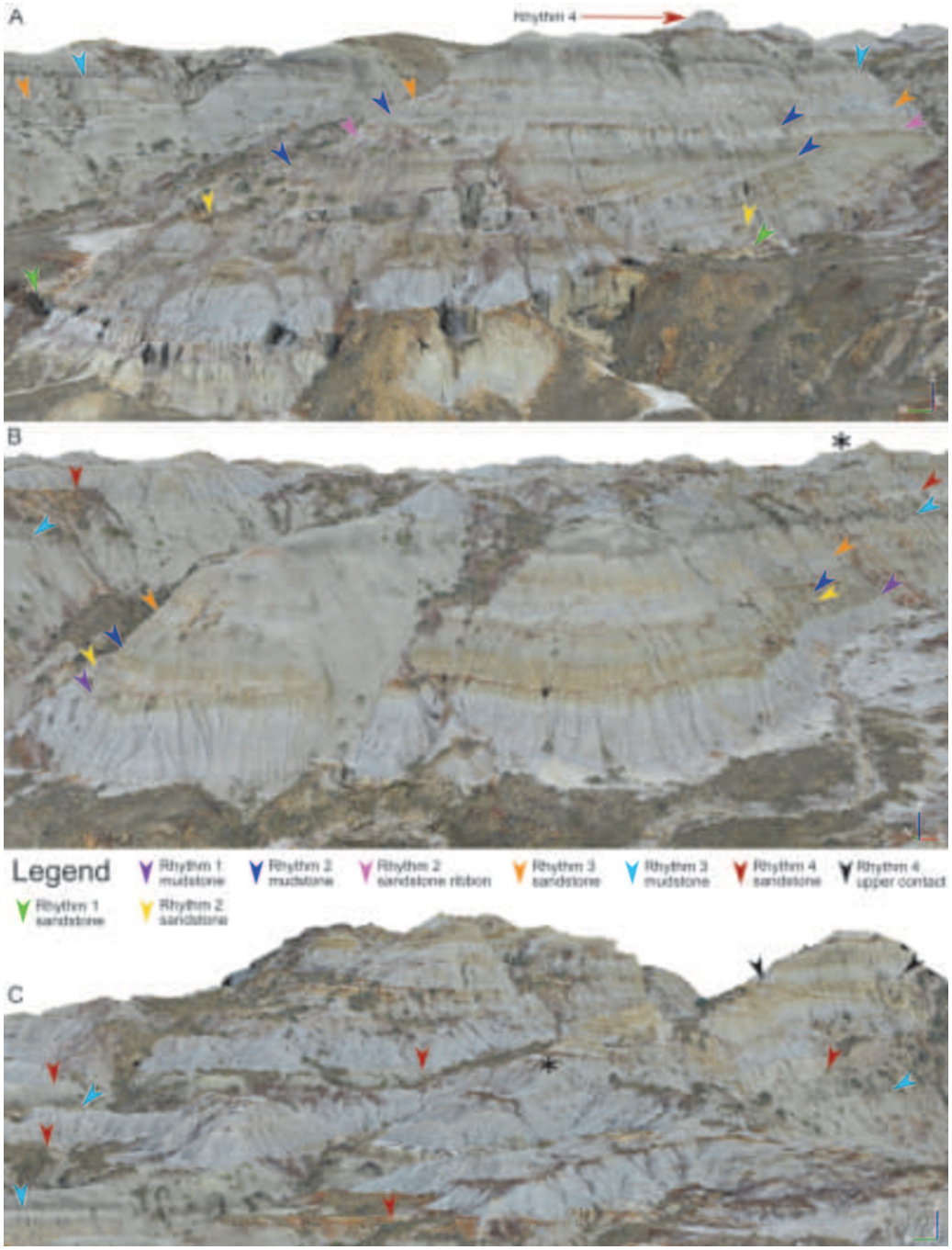

FIGURE 6. Additional renders of digital outcrop model (DOM) highlighting channel cut-and-fill succession in the BB190 Amphitheatre area. A, perspective render of exposure of rill forming southern margin of secondary coulee along which the main stratigraphic section was measured (see Figure 4). Oldman-Dinosaur Park Formation contact marks base of Rhythm 1 sandstone; note change in direction of lateral accretion of ochre siltstone ribbons above and below contact with Rhythm 2 sandstone, as well as laterally discontinuous sandstone ribbon cutting within Rhythm 2 mudstone. B, perspective render of exposure on southern margin of BB190 Amphitheatre area highlighting subtle contact between Rhythms 1 and 2; note Rhythm 2 sandstone downcutting Rhythm 1 mudstone at contact marked by dark red clay-ironstone table. C, orthographic render of uppermost exposures of the Dinosaur Park Formation located upstream from Figure 6B, where the plateau hosting the bonebed narrows into a ridge stretching to the southeast beyond the reaches of the DOM; note possible initiation of a new rhythm at the top of Rhythm 4 with different directions of lateral accretion above and below the proposed contact. Ticks mark bases of each identified lithological unit; black asterisk marks same location in B and C.

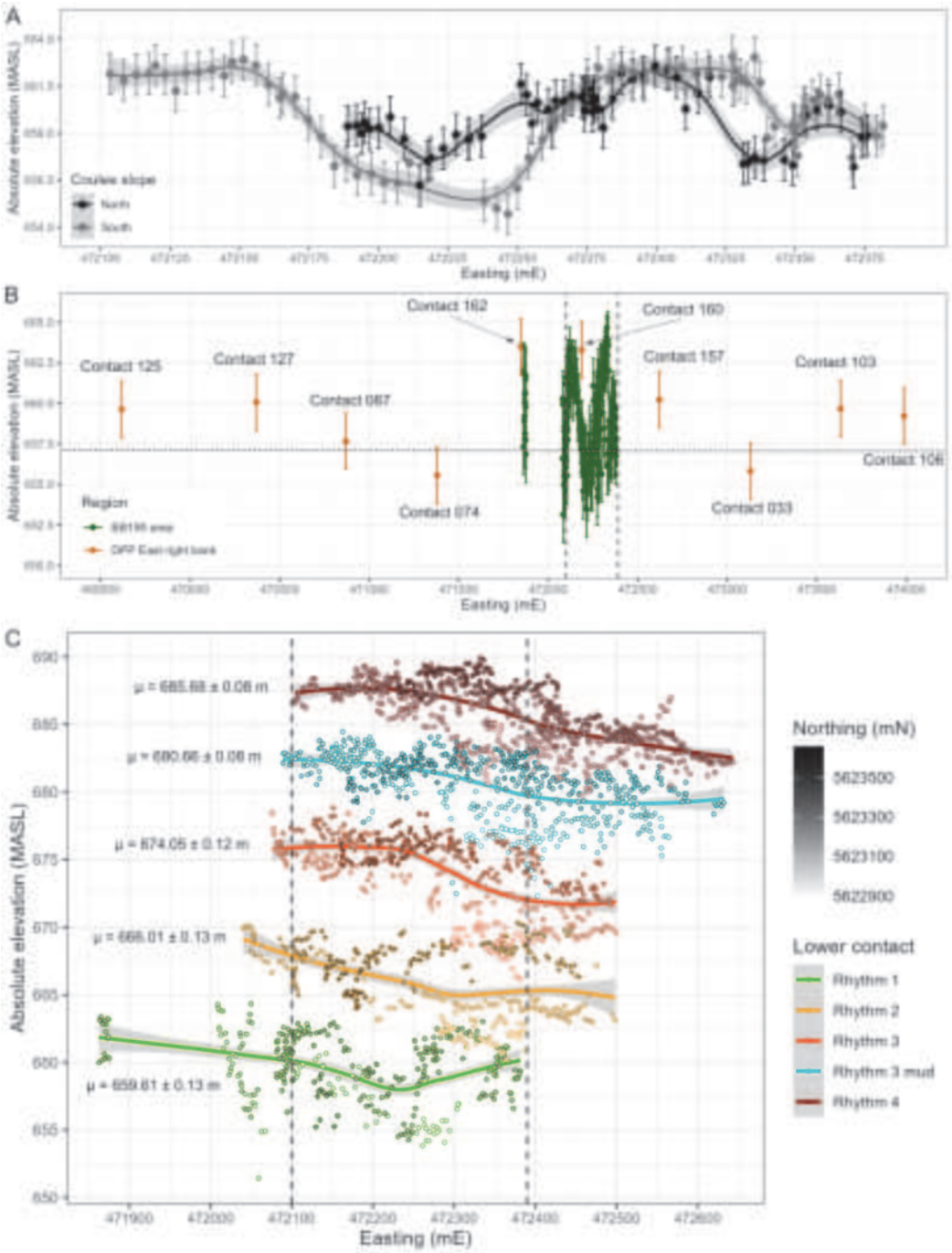

FIGURE 7. Measurement of architectural unit contacts within and beyond BB190 Amphitheatre area. A, measurement of Oldman-Dinosaur Park Formation (OF-DPF) contact elevation solely within a wide coulee forming northern margin of Amphitheatre area; elevation extracted from digital elevation model (DEM) generated during this study and 95% confidence interval of trend curves. B, comparison of OF-DPF contact elevations between aforementioned coulee and all contacts measured along Dinosaur Provincial Park (DPP) eastern right bank during DGPS survey in the early 2000s; elevation for both groups extracted from DEM generated during aerial Lidar survey of DPP. Mean contact elevations with standard errors are as follows: 658.64 ± 0.18 m (BB190 area), 659.46 ± 0.84 m (DPP East right bank). Vertical dashed lines indicate extent of region studied in Figure 7A; horizontal dotted line indicates ~0.05˚ average structural dip of DPP exposures to the northwest. C, comparison of architectural unit lower contacts across BB190 Amphitheatre area. Elevation extracted from DEM generated during this study, with 95% confidence interval of trend curves; vertical dashed lines indicate extent of region studied in Figure 7A; error bars omitted to improve point visibility; standard error provided with mean elevation for each contact.

TABLE 3. Descriptive statistics including standard deviation (σ) and variance (σ^2) for Oldman-Dinosaur Park Formation (ODPF) contact and other architectural unit contacts identified in and around Bonebed 190 Amphitheatre area. Contacts marked in bold were analyzed with digital elevation model (DEM) including entire extent of Dinosaur Provincial Park, provided by Royal Tyrrell Museum of Palaeontology (RMSE ±1.72 m); other contacts analyzed with DEM generated during this study (RMSE ±1.09 m). Elevation range uncertainties are 2*RMSE.

Contact	N sampled points	Elevation (m)					
		Min	Max	Range	Mean	σ	σ^2
OF-DPF (BB190 area, one coulee)*	132	654.70	663.06	8.36 ± 2.18	660.12	1.95	3.81
OF-DPF (BB190 coulee, N slope)	59	656.23	662.56	6.33 ± 2.18	659.79	1.52	2.30
OF-DPF (BB190 coulee, S slope)	73	654.70	663.06	8.36 ± 2.18	660.38	2.22	4.92
OF-DPF (entire BB190 area)	182	653.15	664.67	11.52 ± 3.44	658.64	2.47	6.08
OF-DPF (DPP right bank)	10	655.56	663.48	7.92 ± 3.44	659.46	2.66	7.05
OF-DPF (public loop road)	48	648.21	659.72	11.51 ± 3.44	654.28	2.88	8.31
Rhythm 1 (incl. OF-DPF)	359	651.44	664.33	12.89 ± 2.18	659.61	2.40	5.75
Rhythm 2	366	660.25	670.33	10.08 ± 2.18	666.01	2.49	6.20
Rhythm 3	468	666.18	678.83	12.65 ± 2.18	674.05	2.68	7.19
Rhythm 3 (MUD3)	690	672.29	684.46	12.17 ± 2.18	680.66	2.22	4.91
Rhythm 4	753	679.79	689.92	10.13 ± 2.18	685.68	2.24	5.00

*BB190 Amphitheatre area coulee corresponds to area within black inset in Figure 3

exposures where it is downcut by the overlying Rhythm 2 (Figure 6B). The first trough cross-bedded sandstone (TX1) outcrops at the base of the section for 1.78 m above the OF-DPF contact. TX1 is cut by a siltstone drape reaching a ~2-m thickness in the section's trajectory. The drape then pinches out either side of its maximum depth and is capped by a clay-ironstone intraclast table before being overlain by two additional metres of sandstone. TX1 has a gradational contact with IHS1, which extends upwards for 1.25 m. MUD1 is not clearly visible on the northern outcrop of the coulee where the field section was measured, but it is on the southern one (Figure 4B). The points sampled along Rhythm 1 (including those sampled from the clearly defined Oldman-Dinosaur Park Formation contact) have a mean elevation of ~660 m (Table 3; Figure 7C).

Rhythm 2. Rhythms 1 and 2 were initially considered as a single indivisible architectural unit in the field, but closer examination of the entire DOM revealed that they are distinct. A few outcrops bear a laterally continuous clay-ironstone table that separates a thin underlying mudstone unit (interpreted as MUD1) from an overlying sandstone often laterally accreting into IHS (interpreted as TX2/IHS2) (Figure 6A-B). This lithology suggests an erosional contact where a new channel cut into MUD1, thus initiating a new channel cut-and-fill sequence. Where vertical amalgamation of channel deposits prevents the use of a mudstone bed as a datum (e.g., Figure 5C), changes in direction of lateral accretion can be the only line of evidence for the presence of an erosional contact during digital observations (Figure 6A). Along the stratigraphic section, TX2 has an erosional contact with IHS1 marked by the same clay-ironstone intraclast table found throughout the study area (Figures 4A, 5A-B, 6B). On the northern rill of the coulee, TX2 is only 0.8 m thick before being overlain by MUD2. On the rill forming the southern edge of the stratigraphic section's coulee, TX2 is much deeper and displays extensive lateral accretion into IHS2 as Rhythm 2 downcuts Rhythm 1 (Figure 6A). MUD2 extends for a total of ~4.3 m along the section and is downcut by two channel ribbons: a deeper 1-m thick trough cross-bedded sandstone unit (visible on both sides of the coulee) and a shallower ~0.8-m thick TX unit that appears to accrete laterally into IBS. Such sandstone ribbons are deceptively common within MUD2 along several outcrops of the mapped area: they often appear to represent the base of a new

TABLE 4. Architectural unit depths digitally measured at 20 sections of the BB190 Amphitheatre area based on a high-resolution version of a digital outcrop model (DOM) generated as an Agisoft tiled model through structure-from-motion (SfM) photogrammetry (see Appendix 1). Numbers marked in bold indicate minimum and maximum depths measured.

	Channel cut-and-fill rhythm depth ± internal error (m)				
Section	**Rhythm 1**	**Rhythm 2**	**Rhythm 3**	**Mudstone 3**	**Rhythm 4**
1	8.44 ± 0.58	7.00 ± 0.44	11.65 ± 0.08	4.24 ± 0.08	NA
2	10.33 ± 0.42	8.70 ± 0.05	10.80 ± 0.11	5.69 ± 0.11	NA
3	7.55 ± 0.03	8.80 ± 0.02	12.24 ± 0.05	6.49 ± 0.06	NA
4	8.04 ± 0.05	8.05 ± 0.08	11.00 ± 0.06	4.26 ± 0.03	NA
5	11.54 ± 0.59	9.13 ± 0.06	11.62 ± 0.09	5.68 ± 0.07	NA
6	5.60 ± 0.02	10.71 ± 0.01	12.82 ± 0.05	5.93 ± 0.07	NA
7	5.80 ± 0.06	8.44 ± 0.32	12.18 ± 0.31	5.52 ± 0.06	NA
8	6.45 ± 0.02	10.23 ± 0.04	9.90 ± 0.03	4.57 ± 0.07	NA
9	10.02 ± 0.05 7.22 ± 0.07	6.03 ± 0.41 5.20 ± 0.42	13.58 ± 0.43	5.48 ± 0.39	NA
10	7.55 ± 0.03	8.95 ± 0.59	14.94 ± 0.64	6.93 ± 0.93	NA
11	NA	7.52 ± 0.10	10.97 ± 0.003	3.78 ± 0.06	NA
12	NA	7.50 ± 0.11	11.53 ± 0.11	4.37 ± 0.05	NA
13	NA	8.18 ± 0.96	10.73 ± 0.82	4.35 ± 0.32	NA
14	NA	5.94 ± 0.40	12.45 ± 1.09	5.55 ± 0.71	NA
15	NA	6.95 ± 0.14	14.37 ± 0.13	5.54 ± 0.12	NA
16	NA	7.90 ± 0.04	11.78 ± 0.04	4.99 ± 0.03	NA
17	NA	NA	NA	4.14 ± 0.04	14.49 ± 0.08
18	NA	NA	NA	4.55 ± 0.18	14.29 ± 0.09
19	NA	NA	NA	NA	13.09 ± 0.28
20	10.24 ± 0.03	4.99 ± 0.04	12.23 ± 0.08	4.09 ± 0.09	NA

rhythm, yet they often pinch out laterally (Figures 5A-B, 6A). Across the study area, Rhythm 2 has a lower contact traced for 1,558 m at a mean elevation of ~666 m (Table 3; Figure 7C), with depths ranging from 5.0 to 10.7 m (Table 4).

Rhythm 3. This architectural unit displays the stratigraphic section's most straightforward fining-upward sequence, with a 1.43-m thick TX3 overlain by a ~2.25-m thick IHS3 and then a massive 5.75-m thick MUD3 unit (Figure 4). The contacts between these units are all gradational despite the odd clay-ironstone intraclast table at the TX3-IHS3 contact. Across the study area, Rhythm 3 has a lower contact traced for ~2,004 m at a mean elevation of ~674 m (Table 3; Figure 7C), with depths ranging from 9.9 to 14.9 m (Table 4). MUD3 is thicker, with depths ranging from 3.8 to 6.9 m (Table 4) and is more continuous than the other mudstone units within the mapped area (Figures 3-6). Its lower contact (estimated due to its oft-gradational nature with underlying IHS) is traced for 3,122 m at a mean elevation of ~681 m (Table 3; Figure 7C). Its upper contact (with Rhythm 4, which hosts BB190) has been traced for 3,463 m, at a mean elevation of ~686 m (Table 3; Figure 7C). Since this contact is consistently present across the mapped area and is relatively easy to identify, it constitutes a reliable datum (in addition to the OF-DPF contact) for estimating the relative heights of the fossil quarries explored throughout this project.

Rhythm 4 – the Bonebed 190 host horizon. This unit caps the plateau at the summit of the Bonebed 190 Amphitheatre area, but its entire depth is not preserved in the immediate vicinity of the bonebed due to postglacial erosion (Figure 4B). A closer examination of the sediments hosting BB190 in the vicinity of the main stratigraphic section reveals that a very shallow clay-pebble conglomerate marks the erosional edge between the MUD3 and TX4 units (Figure 4C). This conglomerate is characteristic of a palaeochannel base lag and the most fossil-rich horizon of BB190 lies just above it, at the base of a trough cross-bedded sandstone (TX4) extending for ~7.1 m until a coarse cemented sandstone cap that marks the end of the stratigraphic section. The clay-pebble conglomer-

ate appears to grade into a clay-ironstone table composed of larger nodules at more eastern exposures of the base of Rhythm 4, as seen near the collection sites of fused tyrannosaur nasals and of a tyrannosaur dentary near the original BB190 quarry stake (Figure 8A). The entire depth of Rhythm 4 can only be measured at the eastern extremity of the mapped area, where absolute elevation increases again beyond the BB190 plateau. This is where TX4 fines eastward into IHS4 until it appears to be erosionally overlain by a rhythm that does not sufficiently extend into the mapped area to be traced continuously (Figure 6C). Rhythm 4 has a depth ranging from 13.1 to 14.5 m below this possible contact (Table 4). Therefore, the highest reaches of the mapped area have an absolute elevation of ~702 m, around 44 m above the local OF-DPF contact's mean elevation.

All identified BB190 quarries are traced to the same horizon at the base of TX4: these include the original BB190 locality, which hosts a highly productive vertebrate microsite, as well as the BB190A-C extensions (Figure 8A-G). BB190A, the most extensive macrofossil quarry of the area so far, is notable for its high abundance of ankylosaur remains and its map has been successfully overlain on the orthomosaic to demonstrate that the latter has a sufficiently high resolution for displaying fossil collecting data (Figure 9A-C). BB190B and BB190C have the greatest proximity to the trajectory of the stratigraphic section (Figure 4B), with the latter yielding one of the most impressive specimens of the entire area in the form of a centrosaurine ceratopsid nasal horncore (Figure 8F). BB190C was initially thought to be in a higher horizon than the other quarries since it had a GPS reading ~1.5 m higher than the bonebed horizon base measured a few metres away (Figure 4A-B). However, an examination of its depositional setting confirms that it was formed in the same horizon. An uncollected articulated hadrosaur skeleton consisting of a heavily eroded vertebral series locked in ironstone is also reported just east of BB190's main localities in the same horizon (U197, see Figure 3).

Most of the upper horizons of TX4 do not display any fossil aggregations qualifying as bonebeds, although they have yielded well preserved isolated specimens such as a centrosaurine squamosal, a complete toothless hadrosaur dentary and fused tyrannosaur nasals (Figure 8A-G). The only exception consists of a low-density hadrosaur-dominated bonebed in a narrow coulee, ~1.5 m above the BB190 horizon (BB303, Figure 9D-F). Instead of lying in a channel base lag, most of the bones of BB303 are associated with a sandstone that coarsens upwards into a 20-cm thick clay-ironstone intraclast table extending for around 10 m^2. A few of them were even found within the ironstone lens itself (Figure 9E). This lithological setting is indicative of a very local overbank levee deposit formed during the migration of the TX4 palaeochannel across the surrounding floodplain.

Estimating the stratigraphic position of Bonebeds 190 and 303. A total of seven bonebed and 24 individual fossil specimen localities had their coordinates recorded during the exploration of BB190 (Table 2). Together, they constitute an ideal dataset to investigate the effect of the variation in absolute elevation of architectural unit contacts on the measured stratigraphic positions of individual specimens and bonebeds. First, the effect of the local variability in elevation of the local Oldman-Dinosaur Park Formation contact was assessed by comparing the means and standard deviations of the heights of each marked specimen relative to three different groups of sampled points (Table 2, Figure 10A). Overall, mean heights measured from Contacts 160 and 162 alone were consistently lower than heights based on the 10 points sampled along the same exposure, as well as heights based on 11 more distant points distributed across the entire traced contact (Figure 10B). On the other hand, the mean heights obtained from the latter two groups were almost identical (within ~7 cm). For instance, the BB190A quarry had a mean height of 25.45 m above the groups consisting of Contacts 160 and 162 but mean heights of 28.06 and 27.99 m above the groups consisting of the 10 close contacts and the 11 distant contacts, respectively. However, the standard deviations displayed a different pattern between these three groups: for each locality, the 'Contact 160 and 162' group had a range of ~2.7 m and a standard deviation of 1.89 m; the group of 10 close contacts had a range of ~6.3 m and a standard deviation of 1.94 m; and the group of 10 more distant contacts had a range of ~8.9 m and a standard deviation of 2.95 m. Therefore, the group of 10 OF-DPF contact points sampled along the same coulee had a lower variability in elevation than the group with a similar sample size assembled from scattered exposures of the contact, because the former were far more clustered around their mean (Figure 10B). In fact, the variability of the group restricted to that coulee was more comparable to that observed in the group solely consisting of Contacts 160 and 162, despite having a ~3m difference between their means. A

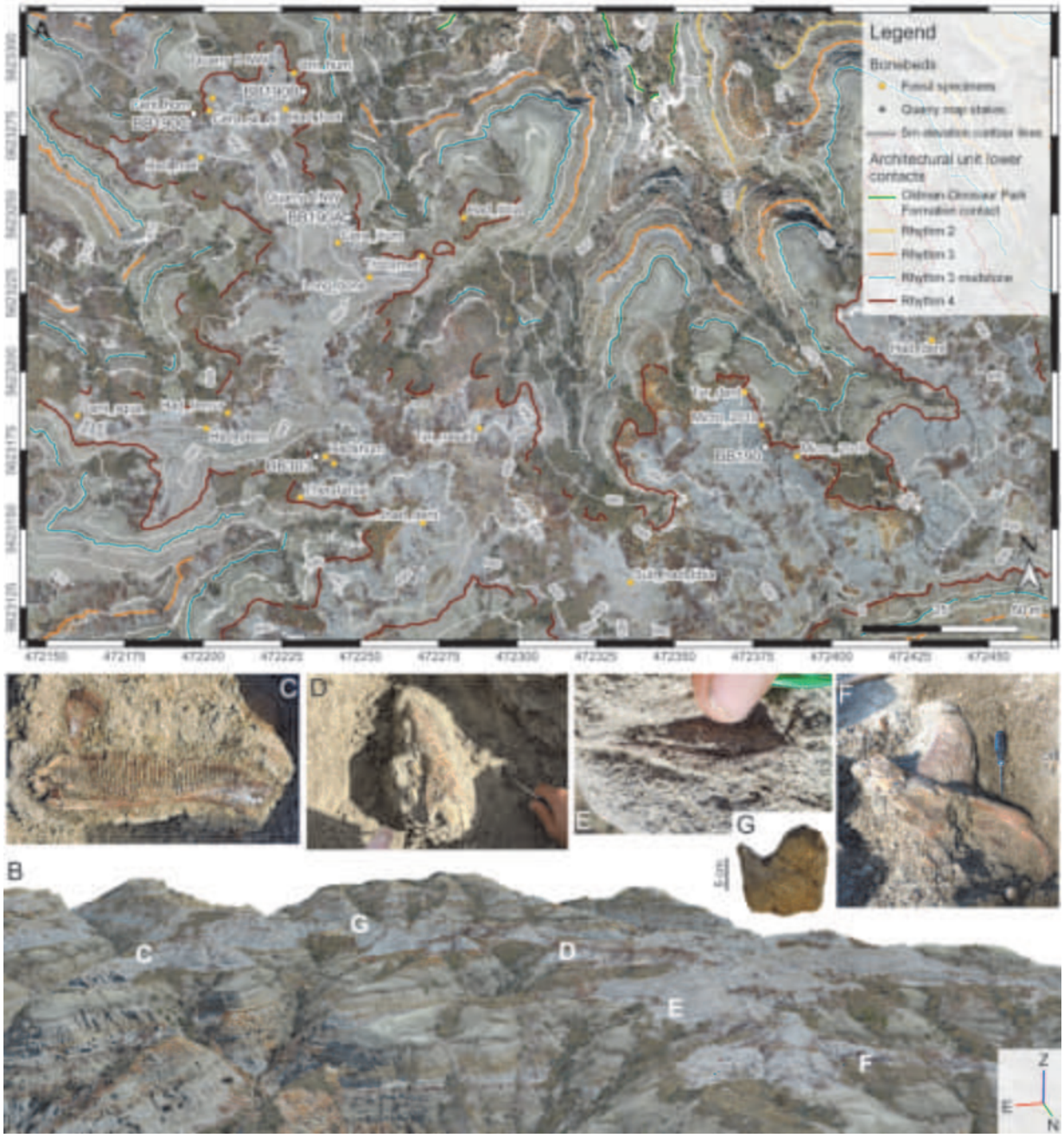

FIGURE 8. Location of significant fossil specimens collected within Bonebed 190 horizon. A, overview of BB190 host horizon within Rhythm 4; 'BB190' point marks original quarry stake marked in 2002; 'BB190A-C' and 'BB303' points mark fossil-rich localities discovered during this study. Coordinates in WGS84 / Universal Transverse Mercator zone 12N, EGM96 geoid. B, location of significant fossil specimens along BB190 horizon at base of Rhythm 4, projected on perspective render of digital outcrop model. C, complete left hadrosaur dentary collected in 2023 near eastern edge of Amphitheatre, ~8m above main BB190 horizon; photo courtesy of Andre Mueller. D, fused tyrannosaur nasals collected in 2023 about halfway between BB190 original quarry height and BB303 quarry height. E, bowfin (family Amiidae) dentary collected in 2022 at BB190A quarry, 10 cm above main bonebed horizon; photo courtesy of Hans Larsson. F, centrosaurine ceratopsid nasal horn core with premaxilla collected in 2018 at BB190C quarry, at northwestern edge of Amphitheatre. G, ceratopsid (cf. *Styracosaurus)* parietal fragment found *ex situ* in 2019 near BB190 microsite.

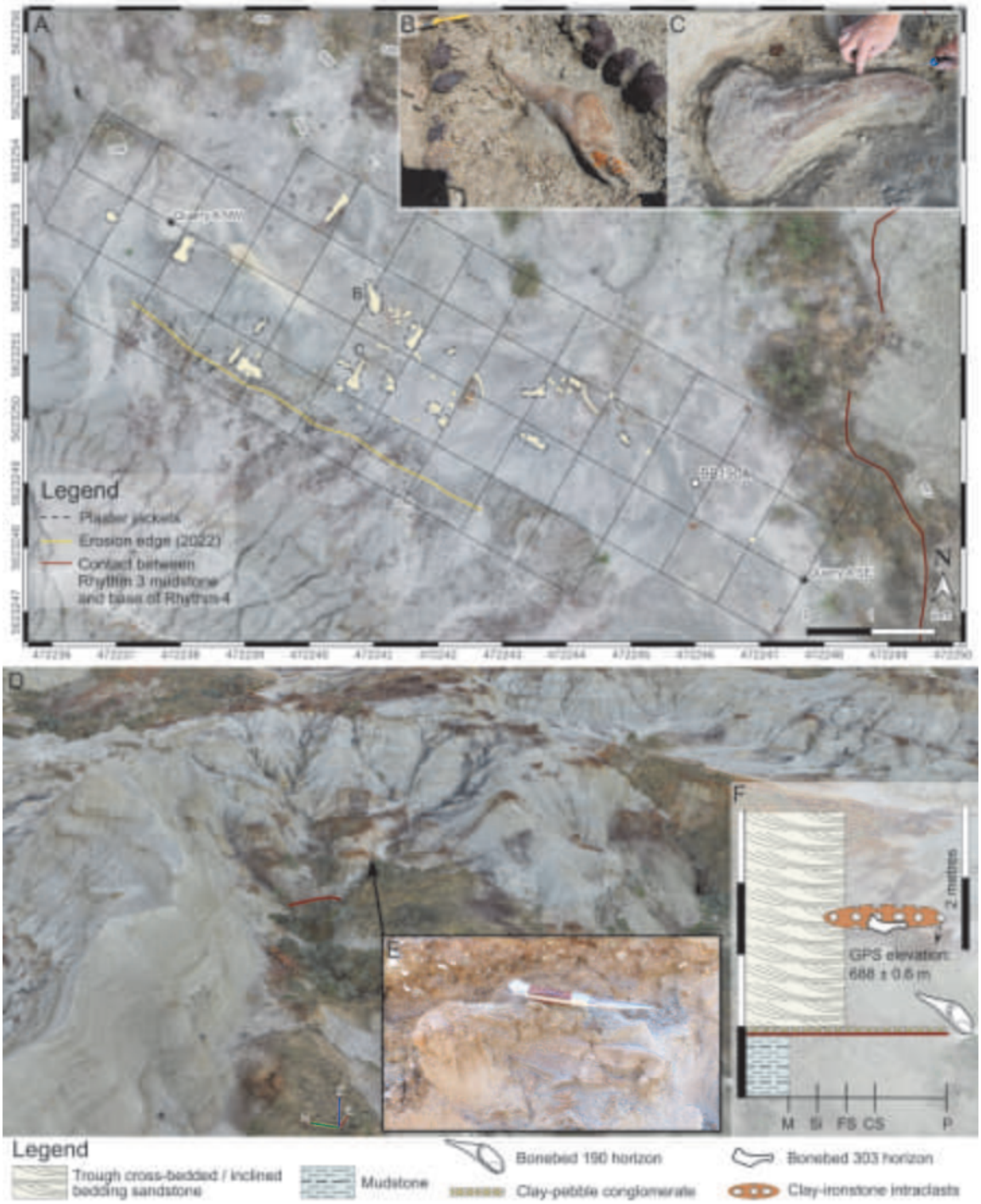

FIGURE 9. Examination of BB190A and BB303 localities. A, BB190A quarry map overlain on orthomosaic. BB190A point represents location of stake for original 2019 quarry map; NW and SE stakes mark corrected 2022 quarry map. B, nodosaurid parascapular spine uncovered from BB190A quarry in 2018. C, nodosaurid left ischium uncovered from BB190A quarry in 2019. Coordinates in WGS84 / Universal Transverse Mercator zone 12N, EGM96 geoid. Quarry and formational contact locations available from database assembled by first author, updated from Currie and Koppelhus (2005). D, perspective render of narrow coulee hosting BB303 locality. E, hadrosaur maxilla found in coarsening upward sandstone at base of clay-ironstone intraclast lens. F, short sedimentary log of BB303; burgundy stroke marks same contact (between MUD3 and Rhythm 4) as in Figure 9D. **Abbreviations: M,** mudstone; **Si,** siltstone; **FS,** fine-grained sandstone; **CS,** coarse-grained sandstone; **P,** pebbles.

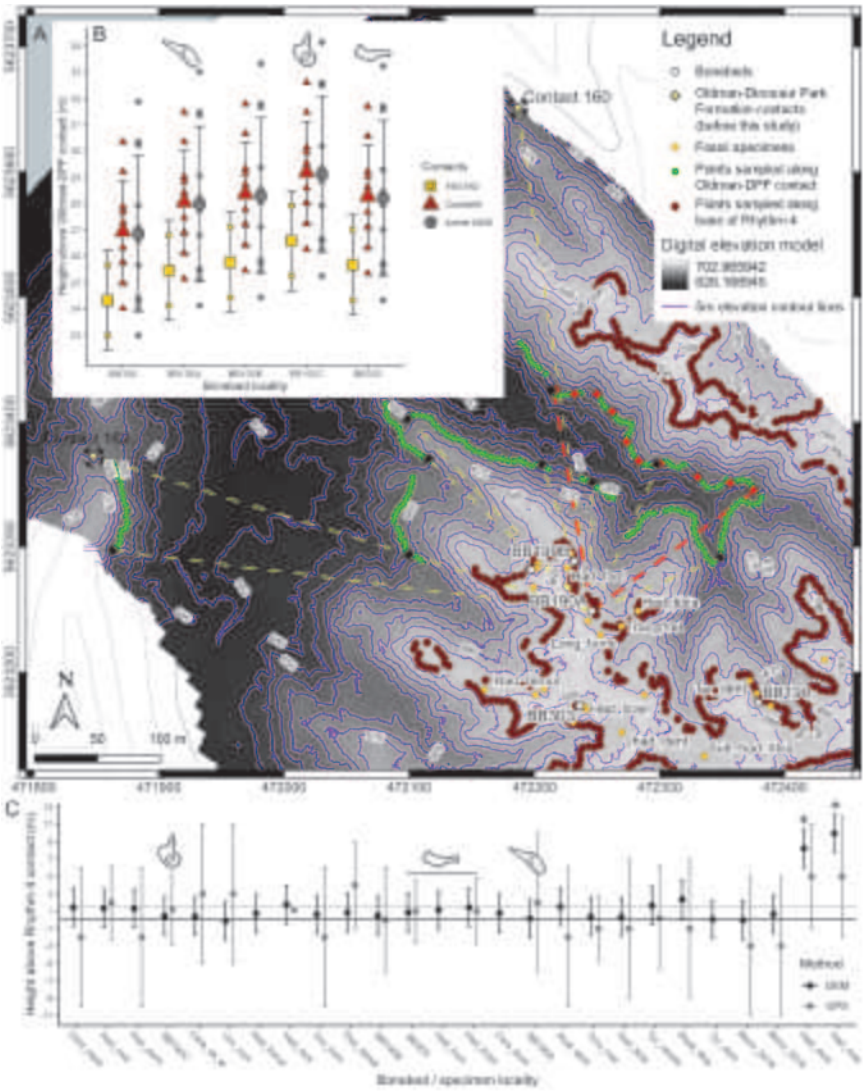

FIGURE 10. Heights of main bonebed quarries and individual fossil specimens above significant architectural unit contacts identified across the BB190 Amphitheatre area. A, location of selected Oldman-Dinosaur Park Formation (OF-DPF) contacts for estimating average specimen/bonebed relative height overlain on digital elevation model (DEM) of study area. Dashed lines connect BB190A (used as example) to all selected contacts; points highlighted in red and yellow represent contacts sampled along point series generated from DEM. Coordinates in WGS84 / Universal Transverse Mercator zone 12N, EGM96 geoid. B, heights above OF-DPF contact estimated from DEM for the five main BB190 quarries identified in this study, based on (1) Contacts 160 and 162 (available from Currie and Koppelhus, 2005); (2) 10 points selected along northern slope of coulee with longest continually preserved OF-DPF contact (red in Figure 10A); (3) 11 contacts selected across entire study area (including Contacts 160 and 162 and additional black points in Figure 10A). Larger points correspond to group means, and error bars represent standard deviations. Point colours in A and B refer to the same groups. C, heights above Rhythm 4 contact for significant bonebed quarries and collected fossil specimens, compared between heights measured with GPS in the field and heights extracted from DEM at nearest point(s) to each specimen along contact polyline traced in QGIS. Dotted line 1.5 m above that marks hypothetical second bonebed layer. Localities ranked by longitude, with the westernmost on the left; notable specimens recovered from BB190A (nodosaurid parascapular spine) and BB190C (centrosaurine nasal horn core) overlie their respective quarry heights; asterisks mark specimens located significantly higher than all others. Note that the same coordinates obtained along the stratigraphic section were used to measure several heights obtained from GPS readings due to lack of raw data, which explains negative values. Specimen and location abbreviations: **Cent_squa,** centrosaurine squamosal; **Cera,** ceratopsid; **Had,** hadrosaurid (adult); **Orn,** ornithomimid; **Jhad,** juvenile hadrosaurid; **Shad,** subadult hadrosaurid; **Ther,** indeterminate theropod; **Troo,** troodontid; **Tyr,** tyrannosaurid; **brain,** braincase; **dent,** dentary; **hum,** humerus; **isch,** ischium; **max,** maxilla; **met,** metatarsal; **sk_el,** skull element; **stern,** sternal plate; **Micro,** microsite points measured in 2018 and 2019.

Kruskal-Wallis test between the three groups produced a *p*-value of 0.2928 (W = 2.4562, df = 2, see Appendices 1 and 3), therefore the null hypothesis of statistically homogeneous means between the three groups was not rejected.

The heights of those same fossil specimens were also compared relative to the base of their host horizon, i.e., the MUD3-Rhythm 4 contact, using field-based and DEM-derived absolute elevations (Figure 10C). For the DEM-derived data, each specimen's height was measured relative to the nearest point sampled along the Rhythm 4 contact. Since those contacts were not always measured in the field, several field-based heights were measured based on the contact that was recorded along the stratigraphic section, which explains occasional negative values for specimens located far from that contact. The use of this alternative datum shows that BB190C falls well within the first 50 cm above the base of Rhythm 4, which means that this quarry was likely part of BB190. However, a more detailed taphonomic study of the Amphitheatre area has yet to be completed to determine whether the BB190C quarry is a result of the same catastrophic or attritional death assemblage as other BB190 quarries. Nonetheless, the DEM-derived heights suggest the presence of a second, far less productive, bone horizon since BB303 and several more isolated specimens fall 1-1.5 m above the channel base (Figure 10C). However, it must be noted that none of the heights reported between the lowest horizon and the proposed slightly upper horizon are statistically significant due to the propagation of absolute elevation errors for each specimen-contact pair. Unsurprisingly, the only two specimens significantly higher than the others are a hadrosaur dentary and a fragmentary maxilla that were collected east of all main quarries of the bonebed.

DISCUSSION

In this project, the BB190 Amphitheatre area proved an ideal palaeoecological study system to investigate three questions concurrently. First, we assessed the impact of the local Oldman-Dinosaur Park Formation contact's absolute elevation variability on the measured stratigraphic position of BB190, along with its biostratigraphic implications for Dinosaur Provincial Park as a whole. Second, we assessed the potential of some architectural units along BB190's stratigraphic succession as marker beds that could be identified along the Park's Belly River Group exposures. Third, we assessed the efficiency of UAV-SfM mapping methods to digitally expand the reconstruction of stratigraphic architecture laterally throughout a relatively broad and complex study area.

The impact of the Oldman-Dinosaur Park Formation contact's elevation variability on stratigraphic distributions

The presence of laterally continuous exposures of the Oldman-Dinosaur Park Formation (OF-DPF) contact at the base of a stratigraphic succession with a mixed faunal bonebed created an opportunity to investigate the extent to which a fossil locality's elevation (and therefore stratigraphic position) relative to that ubiquitous datum can vary in Dinosaur Provincial Park. The OF-DPF contact's elevation was already known to vary by as much as ~30 m over the ~20 km east-west transect of Dinosaur Provincial Park, despite forming an isochronous datum within that same transect. In this respect, one of the key results of the present study is that the OF-DPF contact is now shown to vary substantially by ~10 m (including RMSE) through a single coulee stretching for barely 300 m near Bonebed 190. Relative height estimates for the bonebed's quarries also suggest that the standard deviation associated with the contact's mean elevation increases if that mean is calculated from a high sample size, and that this increase in variability can be tempered if the sample of measurements is located within a single slope of badlands instead of being located across different coulees and buttes. When RMSE is accounted for, the OF-DPF contact's elevation mean and variance (from a ~11.5 m elevation range) observed over a ~600 m east-west transect across the area mapped around that bonebed were not significantly different from the elevation mean and variance (from a ~8 m elevation range) observed across the 10 nearest contacts spread over a ~4.5 km east-west transect along the Red Deer River.

The admittedly low sample size of the latter series prompted us to quantify that elevation variation elsewhere in the Park, this time around the field station and public loop road where the OF-DPF contact was measured at the highest spatial density prior to this study. The elevation range and variance obtained for that sample over a ~2 km east-west transect were found to be very similar to those observed across the BB190 area, which suggests that the important fluctuations in local elevation observed around BB190 are in no way restricted to the eastern reaches of DPP. However, the detection of a statistically lower mean elevation for the contact around the public loop road com-

pared to the BB190 Amphitheatre area (the former being located 8-9 km to the west) was not very surprising, since it confirms previous observations of a structural dip of the Belly River Group's strata to the northwest (Eberth and Hamblin, 1993; Eberth, 2005). These results altogether demonstrate that the OF-DPF contact in the Park can have a similar elevation range on a very local scale to an exposure of the same datum extending on a different spatial order of magnitude. In this way, they confirm a hypothesis that was widely accepted in the geoscience community due to the clear erosional nature of the discontinuity the contact represents (Eberth and Hamblin, 1993; Eberth, 2005; Rogers et al., 2023), but crucially never tested quantitatively until this study. Furthermore, we predict that the frequent peaks and troughs revealed by the detailed tracing of the contact around BB190 will also be detected across the longer transects to which it was compared once the latter are examined in greater detail with a higher density of sampled points, and that this pattern will become ubiquitous across Dinosaur Provincial Park. In this regard, the UAV-SfM photogrammetry method applied in this study has been shown to be a highly promising means of achieving that particular objective. The present confirmation that the OF-DPF contact's elevation can vary by ~10 m along a single coulee among outcrops exhibiting ~0.05º structural dip helps quantify the extent of palaeorelief on the contact's erosional surface. Such an example of channel scouring suggests that many of the oldest channel rhythms ever deposited in the Dinosaur Park Formation were completely downcut by more recent ones.

It is understandable that the previous research focused on the OF-DPF contact so rarely led to a quantification of its local elevation variation because it was conducted with chronostratigraphic objectives in mind, and such variation remains irrelevant at the temporal scale of the geological drivers of the Judith River-Belly River clastic wedge. The only attempt to visualize that pattern occurred as part of an investigation of the geographical and stratigraphic distribution of the Park's dinosaur skeletons (Currie and Russell, 2005). Now, the present study shows that this variation is worth understanding quantitatively among the outcrop locations of this contact in the Western Interior Basin from a palaeontological perspective. This is especially relevant for a system such as DPP that presents such a complete fossil record with strong evidence of turnover in community structure and composition occurring on 10^5-10^6 yr temporal scales, where the currently accepted stratigraphic distributions of species at the foundation of this evidence have been universally derived from individual fossil specimens' heights relative to the OF-DPF contact itself (Brinkman, 1990; Ryan and Evans, 2005; Mallon et al., 2012; Cullen and Evans, 2016; Mallon, 2019; Eberth et al., 2023). A visualization of the maximum possible range in the height of BB190 relative to its nearby OF-DPF exposures in the context of DPP's general stratigraphy shows that this range (including root mean square error propagation) represents ~10% of the Park's entire average outcrop depth and ~12.5% of the average depth of the Dinosaur Park Formation alone (Figure 11). Therefore, the estimated relative height of a given skeleton or bonebed is highly dependent on the location of its referred OF-DPF contact even within a few hundred metres, and several reference points along that contact are ideally recommended to quantify that height uncertainty. It therefore introduces an additional source of error on the stratigraphic position accuracy of any fossil in the Park, which is in the same order of magnitude as the maximum error (14.5 m) calculated from the location of several *Centrosaurus apertus* specimens at the bottom of palaeochannels that downcut underlying sediments (Brown, 2013, Ch.4). It was already acknowledged that the latter source of error could exceed the entire vertical distance of the Park's more constrained observed stratigraphic distributions, such as that of *Styracosaurus albertensis* (Brown, 2013). Now, results from BB190 suggest that these distributions may not be estimated from the OF-DPF contact as accurately as was previously assumed, even after correcting the stratigraphic heights of palaeochannel-hosted specimens. Furthermore, the position error arising from the OF-DPF contact's heterogeneous elevation differs from the error derived from palaeochannel host horizons in two important respects. The first (and more important) one is that the latter error can be corrected relatively easily by identifying the elevation of the upper boundary of a given fossil's host channel cut-and-fill rhythm (which can also vary locally depending on its erosional or gradational nature, see Wood, 1989), while no such simple correction exists regarding the OF-DPF contact. The calculation of descriptive statistics (i.e., mean and standard deviations and errors) for relative height as demonstrated for BB190 may represent the most accurate possible correction in that case, although the uncertainties that linger around it render it unsatisfactory at the temporal scale of the DPF's apparent biotic pat-

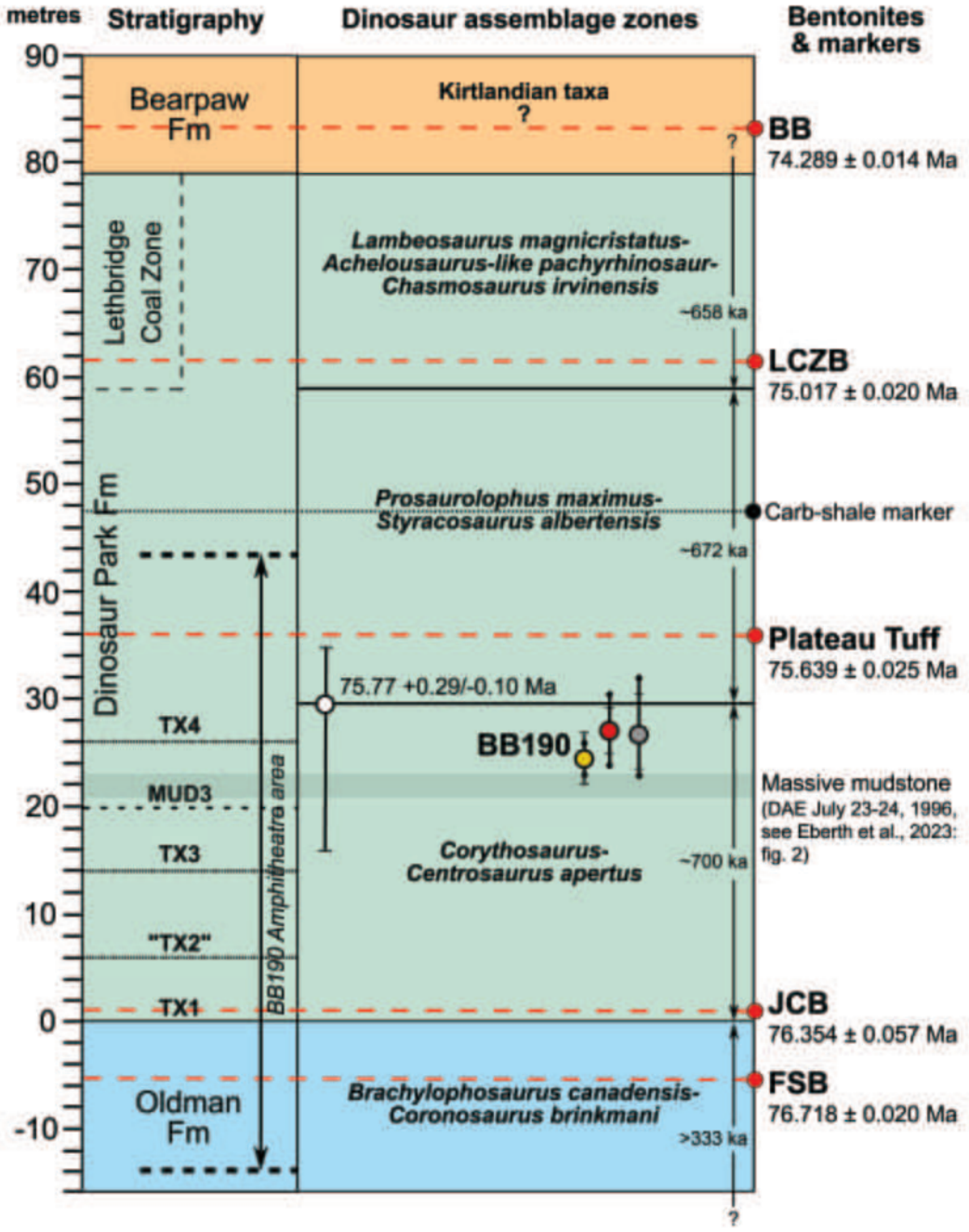

FIGURE 11. Bonebed 190 placed in the litho- and biostratigraphic context of Dinosaur Provincial Park, modified from Eberth et al. (2023). BB190 (original quarry) height above Oldman-Dinosaur Park Formation contact based on three groups of points sampled along contact as in Figure 10B, with mean, minimum and maximum height (as well as error bars representing standard deviations) on display for each group; note that those heights were not corrected for channel downcutting (see Discussion). Thick dashed black lines indicate approximate upper and lower relative height boundaries of mapped area; thinner dashed black lines indicate mean height of lower contact for each architectural unit identified in BB190 Amphitheatre area, MUD3 highlighted among other units' mudstones due to greater potential as a marker bed, TX2 bracketed due to less certain validity as distinct architectural unit (see main text). Radioisotopic age uncertainty of biozone boundary projected on relative height axis based on latest published rock accumulation rates between each bentonite (Eberth et al., 2023). **Abbreviations: BB,** Bearpaw bentonite; **FSB,** Field Station bentonite; **JCB,** Jackson Coulee bentonite; **LCZB,** Lethbridge Coal Zone bentonite; **MUD,** massive mudstone; **TX,** trough cross-bedded sandstone.

terns. Secondly, corrections for channel-hosted specimens will (by definition) always shift their stratigraphic position up-section, while the proposed correction relative to the OF-DPF contact can shift those same positions in either direction, thus being far less predictable.

Contributions of the BB190 survey to the biostratigraphy of the DPF. The resulting uncertainties on the accuracy of stratigraphic distributions in DPP become especially problematic for localities that may be near boundaries of temporal zones defined by biostratigraphy, which often lack any referrable lithostratigraphic datum. BB190 represents an ideal case study to illustrate this additional issue since it was always suspected to lie very close to the proposed boundary between two of the Park's megaherbivorous dinosaur assemblage zones (MAZ-1 and MAZ-2 following Mallon et al., 2012). However, it has only yielded two dinosaur fossils possibly identifiable at the species level to date: the first (found before this study) consists of partial parietals tentatively assigned to *Centrosaurus apertus* based on their overall anatomy but lacking any potentially diagnostic character due to broken parietal processes at both parietal process P1 loci (Sampson et al., 1997; Royal Tyrrell Collections, 2023). The other is a very short parietal fragment that appears to preserve the bases of two large parietal processes very close together (Figure 8G), which is a diagnostic character of *Styracosaurus albertensis*, the centrosaurine ceratopsid taxon consistently hypothesized to succeed to *Centrosaurus* in the Park's chronofauna (Ryan and Evans, 2005; Sampson and Loewen, 2010; Mallon et al., 2012; Mallon, 2019; Eberth et al., 2023). However, the latter specimen was surface collected at the level of the BB190 horizon, which means it could have been washed out of a higher horizon, while the more complete parietals were clearly collected *in situ* from the BB190 original quarry. The discovery of a complete nasal horn core from the bonebed (Figure 8F) only indicates that it belongs to a ceratopsid of the centrosaurine subfamily due to its considerable elongation, but its recurved shape is reported in osteologically mature individuals of both *Centrosaurus* and *Styracosaurus* and therefore provides no information that would be diagnostic at lower taxonomic levels (Ryan et al., 2001, 2007; Sampson et al., 1997). The lack of available biostratigraphic evidence to settle BB190's position between MAZ-1 and MAZ-2 provided an added incentive to estimate it based on the local OF-DPF contact instead. Regardless of the combination of referred points sampled along the contact, the bonebed consistently had an ambiguous position since it always landed within the absolute age uncertainty of the estimated MAZ-1-MAZ-2 boundary (Figure 11). Relative height estimates based on a larger sample size of points selected along the contact only shifted the mean closer to the MAZ-1-MAZ-2 boundary compared to the height estimated solely from the only 2 points measured before this study. The original quarry of BB190 was selected over more recently discovered quarries for Figure 11 since it had the mean relative height with the greatest vertical distance from the MAZ-1-MAZ-2 boundary, and so its elevation range would have been the likeliest to fall within one of these two biozones.

Such lingering uncertainty over the biostratigraphic position of BB190 implies that it (or at least its host horizon) is ideally located to test the megaherbivore turnover hypothesis. The high preservation quality (by bonebed standards) observed in its most complete specimens combined with the high lateral continuity of its host channel horizon raises the possibility of future discoveries, including skeletons preserving more diagnostic features. Indeed, the observed lithology can be interpreted as a channel lag-channel point bar complex, which is the ideal depositional setting for vertebrate skeleton preservation in DPP (Dodson, 1971; Wood et al., 1988; Eberth and Currie, 2005). If future explorations eventually revealed the stratigraphic co-occurrence of species currently assumed to have non-overlapping stratigraphic distributions (e.g., a co-occurrence of *Centrosaurus* and *Styracosaurus* in the same horizon), it would lay the first significant challenge to a paradigm that has prevailed since C.M. Sternberg began investigating geographical and stratigraphic distributions throughout the area nearly 75 years ago (Sternberg, 1950). It might also offer insight into the mode of evolution of those species due to competing hypotheses between cladogenesis (i.e., speciation arising from lineages splitting from a common ancestor) and anagenesis (i.e., speciation occurring along the same lineage), especially in ceratopsians where evidence for anagenesis is more widely reported than in other taxa (Sampson and Loewen, 2010; Scannella et al., 2014; Campbell et al., 2019; Fowler and Fowler, 2020; Wilson et al., 2020). Factors supporting a hypothesis of phyletic evolution (whatever its mode) independent of abiotic conditions as a key driver of megaherbivore turnover in the Belly River Group community (and at least in coeval biotas throughout late Campanian

Laramidia) are (1) a high degree of biogeographical provinciality unparalleled in the Mesozoic Era (despite a relatively equable climate across Laramidia's latitudinal gradient), as well as (2) a stupendously high turnover rate in the DPF largely driven by variation in cranial ornamentation instead of any ecomorphologically relevant characters (Sampson, 1995; Lehman, 2001; Sampson et al., 2010; Mallon and Anderson, 2014; Fowler, 2017; Mallon, 2019). On the other hand, the locations of those biogeographical provinces may well have shifted subtly along that same latitudinal gradient, with each megaherbivore fauna tracking a specific climate and habitat into regions where the Belly River Group is not as well exposed as in DPP. In any case, centrosaurines constitute a textbook example of this biotic turnover pattern since the only characters that are diagnostic of chronologically successive species throughout most of the Belly River Group in that subfamily (i.e., *Coronosaurus brinkmani, Centrosaurus apertus* and *Styracosaurus albertensis*) reside in their parietal frill ornamentation, which is likely to be driven by sexual selection far more than natural selection (Sampson et al., 1997; Ryan and Russell, 2005; Ryan et al., 2007; Frederickson and Tumarkin-Deratzian, 2014). In contrast, the latest Campanian – early Maastrichtian Horseshoe Canyon Formation has three tentative biozones (like the DPF), yet they are spread over at least twice the DPF's duration and appear more reflective of major fluctuations in abiotic conditions (Eberth et al., 2013; Eberth and Kamo, 2020). Furthermore, there is growing evidence that a few DPP species at least have a wider geographical (and likely habitat) range than previously assumed following more sustained exploration of nearby coeval localities, although these range expansions remain on a far lesser spatial scale than prevailing late Campanian dinosaur biogeographical provinces (Chiba et al., 2015; Takasaki et al., 2023; Demers-Potvin and Larsson, 2024). Discussions on the respective influences of ecological and evolutionary drivers of non-avialan dinosaur diversity are especially relevant to the MAZ-1 – MAZ -2 transition (of all faunal assemblage zone boundaries in DPP) since it has even less convincing lithological evidence of a palaeohabitat shift to support ecological replacement, rather than phyletic evolution, as a driver of biotic turnover. The dominant lithology of the DPF broadly shifts from a sandy zone in the lower half of the formation to a muddy zone in its upper half (Eberth, 2005; Eberth et al., 2023), yet that transition roughly postdates the MAZ-1 – MAZ -2 boundary by at least 10 m (Mallon et al., 2012). In any case, this shift in lithology is more accurately indicative of decreased accommodation and corresponding sediment supply over time, which offers very little information on more relevant factors of animal distributions such as floral composition and its derived ecological niche and ecospace predictions.

Contributions of the BB190 survey to the lithostratigraphy of the DPF

In light of the concerns outlined in the previous section regarding the accuracy of any fossil's height relative to the Oldman-Dinosaur Park Formation contact as a reliable proxy of its stratigraphic position, what else can be done to correct the time-averaging of the Dinosaur Provincial Park biota(s) more accurately? Could a more qualitative stratigraphic correlation model be a solution, whereby each quarry is assigned to a sedimentary architectural unit of varying depth regardless of its quantitative relative height? This would undoubtedly reduce the high apparent temporal resolution suggested by height above the OF-DPF contact since fossils found at vertical distances of as much as 14-15 m would realistically be assigned to the same time zone. Conversely, it would render possible time differences between two bonebeds separated by ~1.5 m irrelevant, as in the case of BB303 compared to BB190 in this study. Additionally, it would imply even greater acceptance of time-averaging since these units should necessarily contain at least two of the three major lithofacies types that compose each of the DPF's channel cut-and-fill rhythms (i.e., mudstones, siltstones and trough cross-bedded sandstones) to minimize the risk of taphonomic bias (Wood et al., 1988; Eberth, 1990, 2015; Eberth and Currie, 2005; Brown et al., 2013). Nonetheless, this alternative relative age scale would not be as misleading since it would nullify two of the major sources of stratigraphic position error identified in the Belly River Group, i.e., the variability in OF-DPF contact elevation (this study) and the palaeochannel downcutting effect (Eberth and Getty, 2005; Brown, 2013, Ch.4). Additionally, it would further integrate information on each quarry's depositional environment with information on its stratigraphic positions. These are the theoretical benefits of such an alternative correlation approach, but they would only be attainable if several of these channel cut-and-fill rhythms could be traced individually over a sufficiently long lateral distance to correlate a statistically significant number of quarries, bonebeds and microfossil locali-

ties. Considering the lack of lateral continuity that defines any fluvio-deltaic deposit as opposed to marine or lacustrine deposits (Behrensmeyer and Hook, 1992), this is a tall order indeed. In any case, there remains the intriguing possibility that the duration of deposition represented by each rhythm is actually insignificant on a geological scale, and so that the great depths reached by some of them represent little time-averaging after all. Rock accumulation rates have been estimated for stratigraphic intervals constrained by two bentonite beds that have yielded reliable radioisotopic dates, as in the case of several localities across the Western Interior Basin (see Ramezani et al., 2022; Eberth et al., 2023). However, these fail to account for relatively high sedimentation rates observed in individual fluvio-deltaic deposits (Behrensmeyer, 1982), including some Late Cretaceous palaeochannels located near DPP (Eberth, 1996). If those rates were estimated for some channel cut-and-fill rhythms in DPP (based on palaeocurrent direction and bankfull depths in analogous modern fluvio-deltaic systems), they would likely have a 10^3 – 10^5 yr time resolution for a given depth (Behrensmeyer, 1982), which would be far shorter than the duration obtained by geochronology for a stratigraphic interval of similar depth. This would imply frequent and long-lasting depositional hiatuses throughout the Park's lithostratigraphic succession.

The present study, as well as others (Wood, 1985, 1989; Nesbit et al., 2018), shows that the identification of the Park's main lithofacies (and of the rhythms they compose) can be an effective way of subdividing the Belly River Group's lithostratigraphic succession, at least on a scale of 10^2-10^3 m^2. For example, the sequence stratigraphic correlation of the Cathedral area covered around twice the surface area mapped around BB190 and still led to the identification of six successive rhythms over a vertical distance of 60 m roughly corresponding to the upper two thirds of the DPF (Wood, 1985). That correlation was achieved despite occasional interruptions in some units' lateral continuity caused by the vertical amalgamation of stacked trough cross-bedded sandstones that completely eroded underlying abandoned channel fill mudstone deposits. This complicating factor was observed far less often in the BB190 Amphitheatre area, which led to the identification of four successive rhythms subdividing the lower half of the DPF in that region (Figure 11). Considering that this interval has yielded approximately 80% of all vertebrate fossils known from the DPF in the Park (Eberth and Currie, 2005; Henderson and Tanke, 2010; Brown et al., 2013), an exploration of the lateral continuity of at least some of these units beyond the current study area is recommended in hope of reducing the magnitude of current taphonomic time-averaging. We acknowledge that Rhythm 2 is not as promising a candidate as the other identified units since its contact with the underlying Rhythm 1 was so erosive that it often completely eroded more heterogeneous lithofacies such as MUD1 and could often be detected solely by thin clay-ironstone intraclast layers characteristic of erosional contacts (Wood, 1985). It is likely that Rhythm 2 will eventually be merged with Rhythm 1, which would likely assign the vast majority of the lower DPF's fossil quarries to the same time zone and thus stall potential time-averaging reduction efforts (Eberth and Currie, 2005). In any case, the validity of any of these individual rhythms as regionally significant architectural units would be nullified if a new rhythm that completely downcuts Rhythm 1 all the way to the OF-DPF contact is identified up- or downstream. Under this scenario, the most realistic time zones will likely be composed of stacked palaeochannel deposits.

The most promising candidate marker bed identified in the BB190 Amphitheatre area may not actually be a sandstone, but rather a massive mudstone (MUD3, see Results; Figure 11). It is true that the local elevation of its lower contact is more variable than that of the OF-DPF contact around the bonebed (Table 3), but the location of its upper and lower contacts should still be more constant over long distances than that of downcutting palaeochannel deposits. Furthermore, there is already tentative evidence that it can be correlated in very distant localities of the Park. First, one of the deepest massive mudstone beds identified in the Dinosaur Park Formation type section (measured at the eastern edge of the Park boundaries in the Iddesleigh area) is located 21-23 m above the OF-DPF contact within the same relative height interval as MUD3, although it is roughly 2-3 times thinner in section (Eberth et al., 2023, figure 2). Second, the 'massive shale SH1', which caps the lowest channel rhythm identified in the Cathedral area, might be at the same relative height as MUD3 when accounting for structural dip (Wood, 1985), although this line of evidence is less promising because it is around four times further away from BB190.

Assuming that Rhythms 1 and 2 should form a single time zone and that MUD3 represents a significant marker bed for the DPF of Dinosaur Provincial Park, the ~700 ka of MAZ-1 *(Corythosaurus-*

Centrosaurus apertus) could still be subdivided into 3 sequential time intervals, which represents a resolution unparalleled for fluvial deposits in deep time. Interestingly, the stratigraphic position of massive mudstone MUD3 tentatively coincides with the replacement of *Corythosaurus casuarius* with *Corythosaurus intermedius*, although the latter is very rarely found and thus likely has an underestimated stratigraphic range (Parks, 1923; Mallon, 2019). The sheer depth of MUD3 around BB190 (compared to other mudstones) might simply be explained by a relative lack of local erosion from the overlying coarse member. That said, if it was traced across the entire Park's exposures, it might indicate a period of decreased accommodation and sediment supply in this region of Laramidia's foreland basin and may provide evidence in support of environmental change at the MAZ-1 – MAZ-2 boundary. However, one potential constraint to the correlation of this particular mudstone bed on a more regional scale is that the ratio in vertical proportion of coarse-grained to fine-grained sedimentary members is not consistent within Dinosaur Provincial Park (Wood, 1989): while that ratio oscillates around 3.0 in the Park's south-central area and can be as high as 7.0 in the Cathedral area due to extreme vertical channel amalgamation (Wood, 1985; Visser, 1986), it drops to 0.42 in the Steveville badlands (Koster, 1983). Therefore, MUD3 might be almost impossible to distinguish from similar lithofacies in the latter region, as is already apparent from recent geological surveys (Nesbit et al., 2018; Durkin et al., 2020). Therefore, a broader examination of the sedimentary succession in DPP might still lead us to conclude that the local succession observed in the BB190 Amphitheatre area happens to be easier to interpret than in almost any other region.

Can Dinosaur Provincial Park's time resolution conundrum be solved from the air?

The preceding discussion outlines the necessity to detect common architectural units (or at least marker beds) across the entirety of Dinosaur Provincial Park's exposures as possible solutions to characterize the DPP biota in even greater temporal detail. Considering the huge spatial scale of this exploration and the steep badlands terrain for intensive ground-based excursions, we remain convinced that the future lies in the air, by acquiring images with UAVs in the field, processing them in the lab through SfM photogrammetry, and verifying digital lithofacies identifications with ground-based stratigraphic sections. The aerial survey of the BB190 Amphitheatre area presented in this paper has provided an additional proof of concept for this method, albeit with a slightly different workflow from similar studies in the Park (Nesbit et al., 2018, 2020; Nesbit and Hugenholtz, 2019; Durkin et al., 2020; Mayo et al., 2023). Importantly, we corroborate the results of that previous research showing that UAV flight protocols applied in the field led to reconstructions that had a sufficiently high resolution to digitally identify the DPF's main lithofacies types. An exhaustive exploration of the 3-D digital outcrop model (DOM) and orthomosaic in tandem also provided an efficient assessment of the relevance of each of the lithological units measured in the stratigraphic section to the surrounding alluvial architecture. As an example, some sandstone ribbons would have been indistinguishable from more significant channel belts using the stratigraphic section alone, but their examination in their entirety from contiguous imaged 2-D and 3-D outcrop surfaces greatly facilitated that task. We acknowledge that more sections should have been measured around the bonebed to explore the full potential of ground-based sequence stratigraphic correlation, but that was due to our decision to focus efforts on fossil collection towards a more palaeoecological objective. In addition, the precision of the elevation measurements derived from the root mean square error (RMSE) of the digital elevation model (DEM) obtained from SfM photogrammetry is likely lower than that of measuring staffs used in ground-based stratigraphic mapping, but the latter method has a key precision disadvantage. Its precision may indeed be higher than any remote-sensing approach if a given datum (e.g., the OF-DPF contact) is in close vertical proximity to a given quarry due to a relative lack of measurement error propagation, but that can change quickly if the quarry is located higher in section since those errors will accumulate due to an increasing number of individual measurements with growing vertical distance from the OF-DPF contact. In contrast, the DEM RMSE is (by definition) consistent across the entire mapped area.

From a palaeontological perspective, the identification of the host horizon of BB190 over a relatively large area enabled by SfM photogrammetry constitutes an exciting development in itself. The surface area of the bonebed was estimated at almost 0.1 km^2 from the most distant locations of its known exposed fossils alone. Considering that the same sandstone outcrop extends for considerable distances up- and downriver, BB190 may originally have covered a substantially larger area. In

comparison, the Park's classic *Centrosaurus*-dominated bonebed (BB043) only covers ~0.013 km^2 (Ryan et al., 2001) and the Park's only other well-described multigeneric bonebed to date (BB047) was sampled for fossils over 190 m^2 despite having a more laterally extensive host horizon (Tumarkin-Deratzian, 1997). However, BB190 might not quite have reached the estimated 2.3 km^2 of the Hilda *Centrosaurus* mega-bonebed from the DPF of the South Saskatchewan River (Eberth et al., 2010). Nonetheless, an exhaustive aerial coverage of the Park's exposures combined with accurate GPS readings might provide key evidence to test the lateral extent of several of its bonebeds. This leads us to predict that a remote-sensing approach, combined with a sustained collection of taphonomic data on the ground for individual fossil aggregations (see Brown et al., 2020), will reveal that several localities currently assigned distinct quarry numbers in the Park are in fact part of the same gigantic bonebeds, and so that the Hilda mega-bonebed is not as unusual in its extent. It follows that these bonebeds would constitute valuable additional marker beds for the stratigraphy of the Belly River Group exposed in DPP.

The takeaways from the remote sensing of BB190 are promising, yet there is room for improvement. For instance, the model's absolute geolocation accuracy would likely have been higher if we had used a UAV equipped with real-time kinematics (RTK) or a post-processing kinematics (PPK) module. As it stands, the root mean square error of our ground control points is ±42 cm, but such workflows could potentially reduce it below ±10 cm (e.g., Teppati Losè et al., 2020). At least, the model's relative geolocation accuracy did not appear significantly affected, meaning that it could still provide accurate relative distance measurements irrespective of the precision and accuracy of absolute X, Y and Z coordinates. Consequently, we are now using a different UAV model with PPK capabilities to map a much more extensive territory within DPP as a continuation of the present study (see discussion below). Additionally, incorporating more oblique images on the steep slopes of DPP is known to increase model accuracy (Nesbit and Hugenholtz, 2019). Therefore, the lack of oblique images for most of the mapped area (with the exception of the OF-DPF contact) may have contributed to difficulties in identifying individual bedding planes within the same channel cut-and-fill rhythm, as has been shown elsewhere (Nesbit et al., 2018). A detailed sedimentological study of the bonebed's host horizon would admittedly have offered more insight than relative height measurements alone into the status of fossiliferous layers proposed to represent distinct depositional events from BB190, most notably BB303. It would certainly have reduced the reliance on the tracing of a polyline along an erosional contact that was detected digitally on the orthomosaic, but it is deemed beyond the scope of the present paper. Additionally, some taphonomically relevant facies are simply undetectable from the air (even with a camera with a 40-megapixel sensor resolution) and must still be inspected from the ground, as was the case of the clay-pebble conglomerate that confirmed the formation of BB190 along a palaeochannel lag. It should be noted that several of these thin units are less than 10 cm thick, which reveals a lower resolution limit to the maps produced by UAV-SfM photogrammetry in this study. Ashfall-derived bentonites are yet another lithological facies that can only be distinguished from other mudstones by ground-based observations for now: in fact, it is worth noting that two of the five bentonites currently known from DPP were found by pure serendipity, during sequence stratigraphic correlation of the Cathedral area in the case of the Plateau Tuff (Wood, 1985; Thomas et al., 1990) and during the relatively recent excavation of BB180 in the case of the Jackson Coulee bentonite (Brown et al., 2020). In any case, considerable sedimentological expertise is required to recognize that several of the DPF's erosional contacts might actually be part of the same channel meander belt migration (Nesbit et al., 2018; Durkin et al., 2020). All these caveats show that even the UAV camera with the highest available resolution cannot completely replace ground-based observations, which often provide the context needed to interpret large-scale patterns detected from aerial geological mapping.

As a final limitation, we stress that the data visualization method outlined in this paper is not as practical as it should be. This can partly be explained by our initial emphasis on the orthomosaic as the primary source of digital facies identification due to its efficient integration to 2-D maps in QGIS. However, closer examinations of the outcrops' 3-D structure proved more and more necessary as our understanding of the local stratigraphy increased. For instance, the erosional contact marking Rhythm 2 was only identified once the DOM was inspected in tandem with the orthomosaic. Moreover, channel rhythm depth measurements proved more efficient to obtain by placing manual tie points on the DOM's surface instead of

calculating those depths from absolute heights extracted from two series of points sampled along two successive erosional contacts. The acquisition of outcrop data from the DOM, not just from the DEM and orthomosaic (as was initially planned), may therefore create logistical challenges in terms of geospatial data availability. In future work, we recommend all the vector data be measured from the DOM and subsequently plotted on the same surface in an online repository (e.g., Nesbit et al., 2020), to make the study more interactive and reproducible for viewers and workers who are not as familiar with the terrain of Dinosaur Provincial Park.

The experience acquired during the entire BB190 survey process, from image acquisition and facies observation in the field to digital facies identification from resulting landscape reconstructions, has offered key insights into the best practices to follow as our research group currently begins the creation of a base map covering the entire Park through a similar workflow to the one outlined in this paper, albeit adapted to a far greater spatial scale. In this way, BB190 is strategically located as a starting point for this project due to its well-exposed local OF-DPF contact but also due to its proximity to other potential marker beds. For instance, a thin carbonate shale layer that appears to split the middle DPF hosting the *Prosaurolophus-Styracosaurus* zone into two diachronous units and is interpreted as a precursor of the more common coals of the Lethbridge Coal Zone has reportedly been traced from the Plateau Tuff (in the Cathedral area) eastwards for ~7 km (Eberth, 2005; Eberth et al., 2023). Considering the estimated 75 cm depth of this marker bed and the 2cm/pixel ground resolution of the reconstructions we produced, a more expansive orthomosaic complemented by ground-based observations should result in a powerful visual test of its presence throughout the entire region. If the channel cut-and-fill rhythms discussed above prove insufficiently continuous and this marker bed is shown to have a far more constant variation in elevation than the OF-DPF contact, it could become a very promising alternative datum for estimating stratigraphic distributions. Furthermore, it would evidently be nearer to upper DPF quarries than the OF-DPF contact, which would reduce the propagation of errors derived from ground-based vertical section measurements. A large-scale orthomosaic will also test the continuity of massive mudstone MUD3 (see discussion above) between the DPF type section, through BB190 and all the way to the Cathedral area. Interestingly, a mudstone member of similar depth and stratigraphic position to MUD3 was traced over at least several hundred metres along the outcrops of the Happy Jack's area (across the Red Deer River) during the first tests of UAV mapping on a larger scale (Demers-Potvin, personal obs., 2021). However, its height relative to MUD3 (accounting for structural dip) has yet to be estimated due to relative geolocation inaccuracies and imprecision arising from that preliminary UAV flight protocol. The Iddesleigh area is also known to have the most vertically complete stratigraphic bedrock section in Dinosaur Provincial Park, including the only significant exposures of the Bearpaw Formation in the region (Eberth, 2005). A 3-D and 2-D reconstruction of the region would therefore enable the testing of the consistency of the transition from one of the higher marine shale deposits to the highest underlying tan siltstone bed as a proposed contact between the Lethbridge Coal Zone and the Bearpaw Formation (Brinkman et al., 2005; Eberth et al., 2023). Considering that the Horseshoe Canyon Formation exposed just upstream of DPP displays a more regular succession of visually distinctive coal zones forming laterally extensive marker beds with less vertical mixing of non-contemporaneous strata than in DPP, combined with five distinct bentonites (Quinney et al., 2013; Eberth and Kamo, 2020), a 3-D reconstruction of that sedimentary unit would more likely yield a successful correlation of its fossil localities (Eberth et al., 2013). Nevertheless, the diversity of the DPP community preserved in its fossil assemblage is so exceptional that it provides a sufficient incentive to persist in our current long-term UAV-based mapping project as we strive to further understand the tempo of its ecological (and possibly evolutionary) patterns.

As closing thoughts, it is a promising time to initiate a broader project on the palaeoecology of DPP stemming from the present study considering mounting evidence that biodiversity patterns in deep time are often decoupled between global and local/regional spatial scales (Benson et al., 2021). This implies that relatively well understood individual fossil localities and assemblages are becoming ever more appreciated to answer questions on the long-term persistence of communities in response to perturbations (Barry et al., 1985; DiMichele et al., 2004; Roopnarine and Angielczyk, 2015; Blanco et al., 2021; Roopnarine and Banker, 2021). Therefore, we believe that the DPP biota can contribute substantially to this wider palaeoecological debate as an example of a Late Creta-

ceous North American non-marine community responding to a marine transgression, and that tighter stratigraphic controls on its temporal resolution will only increase its present relevance.

CONCLUSIONS

What began as an essentially exploratory project whose main objective was to assess the geographical extent and palaeodiversity of a mixed faunal bonebed in Dinosaur Provincial Park eventually evolved into a deeper investigation of DPP's entire geological setting through a combination of emerging and enduring technologies. The high fossil discovery rate of the BB190 Amphitheatre area since the renewal of prospection in 2018 suggests that it remains a highly promising study system to investigate the palaeoecology of the Dinosaur Park Formation during a very constrained time span. The present study forms the stratigraphic context for this ongoing project and has concurrently provided two key insights into the temporal resolution of the DPP biota, suggesting that (1) stratigraphic positions solely based on the OF-DPF contact contain major uncertainties even on a local scale and (2) at least some of the channel cut-and-fill rhythms detected in our survey deserve investigation on a broader scale to subdivide the DPF into more lithostratigraphically significant units than the current biostratigraphic frameworks. Together, they represent significant contributions to our understanding of DPP's evolutionary palaeoecology. This project has led to a greater understanding of the benefits and pitfalls of 3-D stratigraphic mapping based on UAV-SfM photogrammetry, which can be applied to characterize outcrops across the world for sedimentology or palaeoecology. It leads to the prediction that the greater spatial overview of the Belly River Group exposed in Dinosaur Provincial Park afforded by the parallel exploration of digital outcrop models (DOMs), digital elevation models (DEMs) and orthomosaics will lead to the distinction of more laterally continuous units as potential marker beds from local units that have hindered solely ground-based stratigraphic correlation attempts. This emerging technology therefore represents one of the most promising solutions to the conundrum surrounding the temporal resolution of the Park's biodiversity patterns.

ACKNOWLEDGEMENTS

The authors of this study wish to acknowledge and highlight that all fieldwork conducted in this study was conducted on the traditional land of the *Niitsítapi* (Blackfoot) peoples, Métis Region 3, and on Treaty 7 land, which includes the traditional territories of the *Siksika, Piikani, Kainai, Tsuut'ina* and *Îyârhe Nakoda* (Stoney Nakota) First Nations. This project would not have been possible without the contributions of all crew members of the 2018, 2019, 2021, 2022 and 2023 editions of the McGill University Vertebrate Palaeontology field course, especially Aidan O. Howenstine, Anthony Smith, Robert Bourque, Hoai-Nam Bui, Anthony Zerafa, Victoria Crozier, José Avila Cervantes, and Luca Larsson. The authors would also like to thank Handling Editor Mathew Stewart, two anonymous reviewers, and Galen Halverson (McGill University) and Corwin Sullivan (University of Alberta) for insightful comments which greatly improved this paper, as well as Caleb Brown (Royal Tyrrell Museum of Palaeontology, TMP), Paul Durkin (University of Manitoba), Jahan Ramezani (MIT), and David Eberth for helpful discussions. Thanks are extended to Allison Vitkus (TMP) for sharing a DEM covering the entirety of Dinosaur Provincial Park and Tim Elrick (Geographic Information Centre, McGill University) for providing software access and data storage, as well as Alberta Parks and Dinosaur Provincial Park for continued research access (Research permits 21-227, 22-022, 23-016 and 23-329), and finally Lane Lucas and Jean Lucas for land access. This research was supported by funding from the Dinosaur Research Institute and doctoral scholarships from the National Science and Engineering Research Council (PGSD3-559424) and the *Fonds de recherche Nature et technologies du Québec* (FRQNT 289816) awarded to AVDP, as well as a Canadian Foundation for Innovation Grant (Project 36146) and NSERC Discovery Grant (RGPIN-2016-06724) awarded to HCEL. This research was conducted as part of AVDP's Ph.D. thesis within the Dinosaur Park Project.

REFERENCES

Barry, J.C., Johnson, N.M., Raza, S.M., and Jacobs, L.L. 1985. Neogene mammalian faunal change in southern Asia: Correlations with climatic, tectonic, and eustatic events. Geology, 13:637–640. https://doi.org/10.1130/0091-7613(1985)13<637:NMFCIS>2.0.CO;2

Behrensmeyer, A.K. 1982. Time resolution in fluvial vertebrate assemblages. Paleobiology, 8:211–227. https://doi.org/10.1017/s0094837300006941

Behrensmeyer, A.K. and Hook, R.W. 1992. Paleoenvironmental contexts and taphonomic modes, p. 15–136. In Behrensmeyer, A.K., Damuth, J.D., DiMichele, W.A., Potts, R., Sues, H.-D., and Wing, S.L. (eds.), Terrestrial Ecosystems through Time. The University of Chicago Press, Chicago.

Behrensmeyer, A.K., Kidwell, S.M., and Gastaldo, R.A. 2000. Taphonomy and paleobiology. Paleobiology, 26:103–147. https://doi.org/10.1017/S0094837300026907

Béland, P. and Russell, D.A. 1978. Paleoecology of Dinosaur Provincial Park (Cretaceous), Alberta, interpreted from the distribution of articulated vertebrate remains. Canadian Journal of Earth Sciences, 15:1012–1024. https://doi.org/10.1139/e78-109

Benson, R.B.J., Butler, R., Close, R.A., Saupe, E., and Rabosky, D.L. 2021. Biodiversity across space and time in the fossil record. Current Biology, 31:R1225–R1236. https://doi.org/10.1016/j.cub.2021.07.071

Blanco, F., Calatayud, J., Martín-Perea, D.M., Domingo, M.S., Menéndez, I., Müller, J., Fernández, M.H., and Cantalapiedra, J.L. 2021. Punctuated ecological equilibrium in mammal communities over evolutionary time scales. Science, 372:300–303. https://doi.org/10.1126/science.abd5110

Bond, C.E., Shipton, Z.K., Jones, R.R., Butler, R.W.H., and Gibbs, A.D. 2007. Knowledge transfer in a digital world: Field data acquisition, uncertainty, visualization, and data management. Geosphere, 3:568–576. https://doi.org/10.1130/GES00094.1

Brinkman, D.B. 1990. Paleoecology of the Judith River Formation (Campanian) of Dinosaur Provincial Park, Alberta, Canada: Evidence from vertebrate microfossil localities. Palaeogeography, Palaeoclimatology, Palaeoecology, 78:37–54. https://doi.org/10.1016/0031-0182(90)90203-J

Brinkman, D.B., Ryan, M.J., and Eberth, D.A. 1998. The paleogeographic and stratigraphic distribution of ceratopsids (Ornithischia) in the upper Judith River Group of Western Canada. Palaios, 13:160–169. https://doi.org/10.2307/3515487

Brinkman, D.B., Braman, D.R., Neuman, A.G., Ralrick, P.E., and Sato, T. 2005. A vertebrate assemblage from the marine shales of the Lethbridge Coal Zone, p. 486–500. In Currie, P.J. and Koppelhus, E.B. (eds.), Dinosaur Provincial Park: A Spectacular Ancient Ecosystem Revealed. Indiana University Press, Bloomington & Indianapolis.

Brown, C.M. 2013. Advances in quantitative methods in dinosaur palaeobiology: a case study in horned dinosaur evolution. Unpublished Ph.D. Thesis, University of Toronto, Toronto, Canada.

Brown, C.M., Evans, D.C., Campione, N.E., O'Brien, L.J., and Eberth, D.A. 2013. Evidence for taphonomic size bias in the Dinosaur Park Formation (Campanian, Alberta), a model Mesozoic terrestrial alluvial?paralic system. Palaeogeography, Palaeoclimatology, Palaeoecology, 372:108–122. https://doi.org/10.1016/j.palaeo.2012.06.027

Brown, C.M., Herridge-Berry, S., Chiba, K., Vitkus, A., and Eberth, D.A. 2020. High-resolution (centimetre-scale) GPS/GIS-based 3D mapping and spatial analysis of in situ fossils in two horned-dinosaur bonebeds in the Dinosaur Park Formation (Upper Cretaceous) at Dinosaur Provincial Park, Alberta, Canada. Canadian Journal of Earth Sciences, 58:225–246. https://doi.org/10.1139/cjes-2019-0183

Campbell, I.A. 1970. Erosion rates in the Steveville Badlands, Alberta. Canadian Geographies / Géographies Canadiennes, 14:202–216. https://doi.org/10.1111/j.1541-0064.1970.tb01568.x

Campbell, J.A., Ryan, M.J., Schröder-Adams, C.J., Holmes, R.B., and Evans, D.C. 2019. Temporal range extension and evolution of the chasmosaurine ceratopsid *'Vagaceratops' irvinensis* (Dinosauria: Ornithischia) in the Upper Cretaceous (Campanian) Dinosaur Park Formation of Alberta. Vertebrate Anatomy Morphology Palaeontology, 7:83–100. https://doi.org/10.18435/vamp29356

Cant, D.J. and Stockmal, G.S. 1989. The Alberta foreland basin: relationship between stratigraphy and cordilleran terrane-accretion events. Canadian Journal of Earth Sciences, 26:1964–1975. https://doi.org/10.1139/e89-166

Chiba, K., Ryan, M.J., Braman, D.R., Eberth, D.A., Scott, E.E., Brown, C.M., Kobayashi, Y., and Evans, D.C. 2015. Taphonomy of a monodominant *Centrosaurus apertus* (Dinosauria: Ceratopsia) bonebed from the Upper Oldman Formation of southeastern Alberta. Palaios, 30:655–667. https://doi.org/10.2110/palo.2014.084

Colomina, I. and Molina, P. 2014. Unmanned aerial systems for photogrammetry and remote sensing: a review. ISPRS Journal of Photogrammetry and Remote Sensing, 92:79–97. https://doi.org/10.1016/j.isprsjprs.2014.02.013

Cullen, T.M. and Evans, D.C. 2016. Palaeoenvironmental drivers of vertebrate community composition in the Belly River Group (Campanian) of Alberta, Canada, with implications for dinosaur biogeography. BMC Ecology, 16:52. https://doi.org/10.1186/s12898-016-0106-8

Cullen, T.M., Zanno, L., Larson, D.W., Todd, E., Currie, P.J., and Evans, D.C. 2021. Anatomical, morphometric, and stratigraphic analyses of theropod biodiversity in the Upper Cretaceous (Campanian) Dinosaur Park Formation. Canadian Journal of Earth Sciences, 58:870–884. https://doi.org/10.1139/cjes-2020-0145

Currie, P.J. and Koppelhus, E.B. 2005. Dinosaur Provincial Park: A Spectacular Ancient Ecosystem Revealed. Indiana University Press, Bloomington & Indianapolis.

Currie, P.J. and Russell, D.A. 2005. The geographic and stratigraphic distribution of articulated and associated dinosaur remains, p. 537–569. In Currie, P.J. and Koppelhus, E.B. (eds.), Dinosaur Provincial Park: A Spectacular Ancient Ecosystem Revealed. Indiana University Press, Bloomington & Indianapolis.

Dawson, F.M., Evans, C.G., Marsh, R., and Richardson, R. 1994. Uppermost Cretaceous and Tertiary strata of the Western Canada sedimentary basin, p. 387–407. In Mossop, G. and Shetsen, I. (eds.), Geological Atlas of the Western Canada Sedimentary Basin. Canadian Society of Petroleum Geologists and the Alberta Research Council, Calgary.

Demers-Potvin, A.V. and Larsson, H.C.E. 2024. Occurrence of *Centrosaurus apertus* (Ceratopsidae: Centrosaurinae) in Saskatchewan, Canada, and expanded dinosaur diversity in the easternmost exposure of the Late Cretaceous (Campanian) Dinosaur Park Formation. Canadian Journal of Earth Sciences, 61:1127-1155. https://doi.org/10.1139/cjes-2023-0125

DiMichele, W.A., Behrensmeyer, A.K, Olszewski, T.D., Labandeira, C.C., Pandolfi, J.M., Wing, S.L., and Bobe, R. 2004. Long-term stasis in ecological assemblages: evidence from the fossil record. Annual Review of Ecology, Evolution, and Systematics, 35:285–322. https://doi.org/10.1146/annurev.ecolsys.35.120202.110110

Dinosaur Provincial Park World Heritage Site. 2013. [Map]. Parks Division, Alberta Tourism, Parks and Recreation. https://whc.unesco.org/en/documents/140204/

Dodson, P. 1971. Sedimentology and taphonomy of the Oldman Formation (Campanian), Dinosaur Provincial Park, Alberta (Canada). Palaeogeography, Palaeoclimatology, Palaeoecology, 10:21–74. https://doi.org/10.1016/0031-0182(71)90044-7

Durkin, P.R., Hubbard, S.M., Holbrook, J., Weleschuk, Z., Nesbit, P., Hugenholtz, C., Lyons, T., and Smith, D.G. 2020. Recognizing the product of concave-bank sedimentary processes in fluvial meander-belt strata. Sedimentology, 67:2819–2849. https://doi.org/10.1111/sed.12743

Eberth, D.A. 1990. Stratigraphy and sedimentology of vertebrate microfossil sites in the uppermost Judith River Formation (Campanian), Dinosaur Provincial Park, Alberta, Canada.

Palaeogeography, Palaeoclimatology, Palaeoecology, 78:1–36. https://doi.org/10.1016/0031-0182(90)90202-I

Eberth, D.A. 1996. Origin and significance of mud-filled incised valleys (Upper Cretaceous) in southern Alberta, Canada. Sedimentology, 43:459–477. https://doi.org/10.1046/j.1365-3091.1996.d01-15.x

Eberth, D.A. 2005. The geology, p. 54–82. In Currie, P.J. and Koppelhus, E.B. (eds.), Dinosaur Provincial Park: A Spectacular Ancient Ecosystem Revealed. Indiana University Press, Bloomington & Indianapolis.

Eberth, D.A. 2015. Origins of dinosaur bonebeds in the Cretaceous of Alberta, Canada. Canadian Journal of Earth Sciences, 52:655–681. https://doi.org/10.1139/cjes-2014-0200

Eberth, D.A. 2024. Stratigraphic architecture of the Belly River Group (Campanian, Cretaceous) in the plains of southern Alberta: revisions and updates to an existing model and implications for correlating dinosaur-rich strata. PLOS ONE, 19:e0292318. https://doi.org/10.1371/journal.pone.0292318

Eberth, D.A. and Currie, P.J. 2005. Vertebrate taphonomy and taphonomic modes, p. 453–477. In Currie, P.J. and Koppelhus, E.B. (eds.), Dinosaur Provincial Park: A Spectacular Ancient Ecosystem Revealed. Indiana University Press, Bloomington & Indianapolis.

Eberth, D.A. and Getty, M.A. 2005. Ceratopsian bonebeds: occurrence, origins, and significance, p. 501–536. In Currie, P.J. and Koppelhus, E.B. (eds.), Dinosaur Provincial Park: A Spectacular Ancient Ecosystem Revealed. Indiana University Press, Bloomington & Indianapolis.

Eberth, D.A. and Hamblin, A.P. 1993. Tectonic, stratigraphic, and sedimentologic significance of a regional discontinuity in the upper Judith River Group (Belly River wedge) of southern Alberta, Saskatchewan, and northern Montana. Canadian Journal of Earth Sciences, 30:174–200. https://doi.org/10.1139/e93-016

Eberth, D.A. and Kamo, S.L. 2020. High-precision U–Pb CA–ID–TIMS dating and chronostratigraphy of the dinosaur-rich Horseshoe Canyon Formation (Upper Cretaceous, Campanian–Maastrichtian), Red Deer River valley, Alberta, Canada. Canadian Journal of Earth Sciences, 57:1220–1237. https://doi.org/10.1139/cjes-2019-0019

Eberth, D.A., Brinkman, D.B., and Barkas, V. 2010. A centrosaurine mega-bonebed from the Upper Cretaceous of southern Alberta: implications for behavior and death events, p. 495-508. In Ryan, M.J., Chinnery-Allgeier, B.J., and Eberth, D.A. (eds.), New Perspectives on Horned Dinosaurs. Indiana University Press, Bloomington & Indianapolis.

Eberth, D.A., Evans, D.C., Brinkman, D.B., Therrien, F., Tanke, D.H., and Russell, L.S. 2013. Dinosaur biostratigraphy of the Edmonton Group (Upper Cretaceous), Alberta, Canada: evidence for climate influence. Canadian Journal of Earth Sciences, 50:701–726. https://doi.org/10.1139/cjes-2012-0185

Eberth, D.A., Evans, D.C., and Lloyd, D.W.H. 2015. Occurrence and taphonomy of the first documented hadrosaurid bonebed from the Dinosaur Park Formation (Belly River Group, Campanian) at Dinosaur Provincial Park, Alberta, Canada, p. 502–523. In Eberth, D.A. and Evans, D.C. (eds.), Hadrosaurs. Indiana University Press, Bloomington & Indianapolis.

Eberth, D.A., Evans, D.C., Ramezani, J., Kamo, S.L., Brown, C.M., Currie, P.J., and Braman, D.R. 2023. Calibrating geologic strata, dinosaurs, and other fossils at Dinosaur Provincial Park (Alberta, Canada) using a new CA-ID-TIMS U–Pb geochronology. Canadian Journal of Earth Sciences, 60:1627–1646. https://doi.org/10.1139/cjes-2023-0037

Evans, D.C., McGarrity, C.T., and Ryan, M.J. 2015. A skull of *Prosaurolophus maximus* from southeastern Alberta and the spatiotemporal distribution of faunal zones in the Dinosaur Park Formation, p. 200–207. In Eberth, D.A. and Evans, D.C. (eds.), Hadrosaurs. Indiana University Press, Bloomington & Indianapolis.

Evans, D.J.A. 2000. Quaternary geology and geomorphology of the Dinosaur Provincial Park area and surrounding plains, Alberta, Canada: the identification of former glacial lobes, drainage diversions and meltwater flood tracks. Quaternary Science Reviews, 19:931–958. https://doi.org/10.1016/S0277-3791(99)00029-3

Fanti, F., Cantelli, L., and Angelicola, L. 2018. High-resolution maps of Khulsan and Nemegt localities (Nemegt Basin, southern Mongolia): stratigraphic implications. Palaeogeography,

Palaeoclimatology, Palaeoecology, 494:14–28. https://doi.org/10.1016/j.palaeo.2017.10.015

Fanti, F., Cantelli, L., Currie, P.J., Funston, G.F., Cenni, N., Catellani, S., Chinzorig, T., Tsogtbaatar, K.H., and Barsbold, R. 2024. High-resolution UAV maps of the Gobi Desert provide new insights into the Upper Cretaceous of Mongolia. Cretaceous Research, 161:105916. https://doi.org/10.1016/j.cretres.2024.105916

Fowler, D.W. 2017. Revised geochronology, correlation, and dinosaur stratigraphic ranges of the Santonian-Maastrichtian (Late Cretaceous) formations of the Western Interior of North America. PLOS ONE, 12:e0188426. https://doi.org/10.1371/journal.pone.0188426

Fowler, D.W. and Fowler, E.A.F. 2020. Transitional evolutionary forms in chasmosaurine ceratopsid dinosaurs: evidence from the Campanian of New Mexico. PeerJ, 8:e9251. https://doi.org/10.7717/peerj.9251

Frederickson, J.A. and Tumarkin-Deratzian, A.R. 2014. Craniofacial ontogeny in *Centrosaurus apertus*. PeerJ, 2:e252. https://doi.org/10.7717/peerj.252

Hamblin, A.P. 1997. Regional distribution and dispersal of the Dinosaur Park Formation, Belly River Group, surface and subsurface of southern Alberta. Bulletin of Canadian Petroleum Geology, 45:377–399.

Hamblin, A.P. and Abrahamson, B.W. 1996. Stratigraphic architecture of “basal Belly River” cycles, Foremost Formation, Belly River Group, subsurface of southern Alberta and southwestern Saskatchewan. Bulletin of Canadian Petroleum Geology, 44:654–673.

Henderson, D.M. and Tanke, D.H. 2010. Estimating past and future dinosaur skeletal abundances in Dinosaur Provincial Park, Alberta, Canada. Canadian Journal of Earth Sciences, 47:1291–1304. https://doi.org/10.1139/E10-033

Koster, E.H. 1983. Sedimentology of the Upper Cretaceous Judith River (Belly River) Formation, Dinosaur Provincial Park, Alberta. Canadian Society of Petroleum Geologists Conference.

Koster, E.H., Currie, P.J., Eberth, D.A., Brinkman, D.B., Johnston, P.A., and Braman, D.R. 1987. Sedimentology and Palaeontology of the Upper Cretaceous Judith River/Bearpaw Formations at Dinosaur Provincial Park, Alberta. Geological Association of Canada, Mineralogical Association of Canada, Joint Annual Meeting.

Lambe, L.M. 1913. A new genus and species of Ceratopsia from the Belly River Formation of Alberta. The Ottawa Naturalist, 27:109–116.

Lehman, T.M. 2001. Late Cretaceous dinosaur provinciality, p. 310–328. In Tanke, D.H. and Carpenter, K. (eds.), Mesozoic Vertebrate Life. Indiana University Press, Bloomington & Indianapolis.

Lowi-Merri, T.M. and Evans, D.C. 2020. Cranial variation in *Gryposaurus* and biostratigraphy of hadrosaurines (Ornithischia: Hadrosauridae) from the Dinosaur Park Formation of Alberta, Canada. Canadian Journal of Earth Sciences, 57:765–779. https://doi.org/10.1139/cjes-2019-0073

Mallon, J.C. 2019. Competition structured a Late Cretaceous megaherbivorous dinosaur assemblage. Scientific Reports, 9:15447. https://doi.org/10.1038/s41598-019-51709-5

Mallon, J.C. and Anderson, J.S. 2014. Implications of beak morphology for the evolutionary paleoecology of the megaherbivorous dinosaurs from the Dinosaur Park Formation (upper Campanian) of Alberta, Canada. Palaeogeography, Palaeoclimatology, Palaeoecology, 394:29–41. https://doi.org/10.1016/j.palaeo.2013.11.014

Mallon, J.C., Evans, D.C., Ryan, M.J., and Anderson, J.S. 2012. Megaherbivorous dinosaur turnover in the Dinosaur Park Formation (upper Campanian) of Alberta, Canada. Palaeogeography, Palaeoclimatology, Palaeoecology, 350–352:124–138. https://doi.org/10.1016/j.palaeo.2012.06.024

Mayo, K., Silva, R.L., and Durkin, P.R. 2023. Paleoenvironmental reconstruction of Late Cretaceous rivers, Dinosaur Park Formation, Alberta, Canada. Sedimentary Geology, 457:106499. https://doi.org/10.1016/j.sedgeo.2023.106499

Nesbit, P.R. and Hugenholtz, C.H. 2019. Enhancing UAV–SfM 3D model accuracy in high-relief landscapes by incorporating oblique images. Remote Sensing, 11:239. https://doi.org/10.3390/rs11030239

Nesbit, P.R., Durkin, P.R., Hugenholtz, C.H., Hubbard, S.M., and Kucharczyk, M. 2018. 3-D stratigraphic mapping using a digital outcrop model derived from UAV images and structure-from-motion photogrammetry. Geosphere, 14:2469–2486. https://doi.org/10.1130/GES01688.1

Nesbit, P.R., Boulding, A., Hugenholtz, C., Durkin, P., and Hubbard, S. 2020. Visualization and sharing of 3D digital outcrop models to promote open science. GSA Today, 30:4–10. https://doi.org/10.1130/GSATG425A.1

Nopcsa, F. 1928. Palaeontological notes on reptiles. Geologica Hungarica, Seria Palaeontologica, 1:1-84.

Parks, W.A. 1923. *Corythosaurus intermedius,* a New Species of Trachodont Dinosaur (University of Toronto Studies, Geological Series 15). University Library.

Pavlis, T.L. and Mason, K.A. 2017. The new world of 3D geologic mapping. GSA Today, 27:4–10. https://doi.org/10.1130/GSATG313A.1

Quinney, A., Therrien, F., Zelenitsky, D.K., and Eberth, D.A. 2013. Palaeoenvironmental and palaeoclimatic reconstruction of the Upper Cretaceous (late Campanian–early Maastrichtian) Horseshoe Canyon Formation, Alberta, Canada. Palaeogeography, Palaeoclimatology, Palaeoecology, 371:26–44. https://doi.org/10.1016/j.palaeo.2012.12.009

R Core Team. 2023. R: A language and environment for statistical computing. R Foundation for Statistical Computing, Vienna, Austria. https://www.R-project.org/

Ramezani, J., Beveridge, T.L., Rogers, R.R., Eberth, D.A., and Roberts, E.M. 2022. Calibrating the zenith of dinosaur diversity in the Campanian of the Western Interior Basin by CA-ID-TIMS U–Pb geochronology. Scientific Reports, 12:16026. https://doi.org/10.1038/s41598-022-19896-w

Rogers, R.R., Eberth, D.A., and Ramezani, J. 2023. The “Judith River−Belly River problem” revisited (Montana-Alberta-Saskatchewan): new perspectives on the correlation of Campanian dinosaur-bearing strata based on a revised stratigraphic model updated with CA-ID-TIMS U-Pb geochronology. GSA Bulletin, 136:1221–1237. https://doi.org/10.1130/B36999.1

Roopnarine, P.D. and Angielczyk, K.D. 2015. Community stability and selective extinction during the Permian-Triassic mass extinction. Science, 350:90–93. https://doi.org/10.1126/science.aab1371

Roopnarine, P.D. and Banker, R.M.W. 2021. Ecological stasis on geological time scales. Science, 372:237–238. https://doi.org/10.1126/science.abh2853

Royal Tyrrell Collections. 2023. TMP2005.009.0069. https://rtmp.emuseum.com/objects/141713/tmp20050090069

Russell, L.S. 1966. Dinosaur hunting in Western Canada. Royal Ontario Museum Life Sciences Contributions, 70:1–37. https://doi.org/10.5962/bhl.title.52089

Ryan, M.J. and Evans, D.C. 2005. Ornithischian dinosaurs, p. 312–348. In Currie, P.J. and Koppelhus, E.B. (eds.), Dinosaur Provincial Park: A Spectacular Ancient Ecosystem Revealed. Indiana University Press, Bloomington & Indianapolis.

Ryan, M.J. and Russell, A.P. 2005. A new centrosaurine ceratopsid from the Oldman Formation of Alberta and its implications for centrosaurine taxonomy and systematics. Canadian Journal of Earth Sciences, 42:1369–1387. https://doi.org/10.1139/e05-029

Ryan, M.J., Russell, A.P., Eberth, D.A., and Currie, P.J. 2001. The taphonomy of a *Centrosaurus* (Ornithischia: Ceratopsidae) bone bed from the Dinosaur Park Formation (Upper Campanian), Alberta, Canada, with comments on cranial ontogeny. Palaios, 16:482–506. https://doi.org/10.1669/0883-1351(2001)016<0482:TTOACO>2.0.CO;2

Ryan, M.J., Holmes, R., and Russell, A.P. 2007. A revision of the late Campanian centrosaurine ceratopsid genus *Styracosaurus* from the Western Interior of North America. Journal of Vertebrate Paleontology, 27:944–962. https://doi.org/10.1671/0272-4634(2007)27[944:AROTLC]2.0.CO;2

Ryan, M.J., Eberth, D.A., Brinkman, D.B., Currie, P.J., and Tanke, D.H. 2010. A new *Pachyrhinosaurus*-like ceratopsid from the upper Dinosaur Park Formation (late Campanian)

of southern Alberta, Canada, p. 141–155. In Ryan, M.J., Chinnery-Allgeier, B.J., and Eberth, D.A. (eds.), New Perspectives on Horned Dinosaurs. Indiana University Press, Bloomington & Indianapolis.

Sampson, S.D. 1995. Two new horned dinosaurs from the Upper Cretaceous Two Medicine Formation of Montana; with a phylogenetic analysis of the Centrosaurinae (Ornithischia: Ceratopsidae). Journal of Vertebrate Paleontology, 15:743–760. https://doi.org/10.1080/02724634.1995.10011259

Sampson, S.D. and Loewen, M.A. 2010. Unraveling a radiation: a review of the diversity, stratigraphic distribution, biogeography, and evolution of horned dinosaurs (Ornithischia: Ceratopsidae), p. 405–427. In Ryan, M.J., Chinnery-Allgeier, B.J., and Eberth, D.A. (eds.), New Perspectives on Horned Dinosaurs. Indiana University Press, Bloomington & Indianapolis.

Sampson, S.D., Ryan, M.J., and Tanke, D.H. 1997. Craniofacial ontogeny in centrosaurine dinosaurs (Ornithischia: Ceratopsidae): taxonomic and behavioral implications. Zoological Journal of the Linnean Society, 121:293–337. https://doi.org/10.1111/j.1096-3642.1997.tb00340.x

Sampson, S.D., Loewen, M.A., Farke, A.A., Roberts, E.M., Forster, C.A., Smith, J.A., and Titus, A.L. 2010. New horned dinosaurs from Utah provide evidence for intracontinental dinosaur endemism. PLOS ONE, 5:e12292. https://doi.org/10.1371/journal.pone.0012292

Scannella, J.B., Fowler, D.W., Goodwin, M.B., and Horner, J.R. 2014. Evolutionary trends in *Triceratops* from the Hell Creek Formation, Montana. Proceedings of the National Academy of Sciences, 111:10245–10250. https://doi.org/10.1073/pnas.1313334111

Sternberg, C.H. 1917. Hunting Dinosaurs in the Bad Lands of the Red Deer River, Alberta, Canada. World Company Press, Lawrence, Kansas.

Sternberg, C.M. 1950. Steveville west of the 4th meridian, with notes on fossil localities [Map]. Geological Survey of Canada, Topographic Map 969A.

Takasaki, R., Chiba, K., Fiorillo, A.R., Brink, K.S., Evans, D.C., Fanti, F., Saneyoshi, M., Maltese, A., and Ishigaki, S. 2023. Description of the first definitive *Corythosaurus* (Dinosauria, Hadrosauridae) specimens from the Judith River Formation in Montana, USA and their paleobiogeographical significance. The Anatomical Record, 306:1918–1938. https://doi.org/10.1002/ar.25097

Teppati Losè, L., Chiabrando, F., and Giulio Tonolo, F. 2020. Are measured ground control points still required in UAV based large scale mapping? Assessing the positional accuracy of an RTK multi-rotor platform. The International Archives of the Photogrammetry. Remote Sensing and Spatial Information Sciences., XLIII-B1-2020:507–514. https://doi.org/10.5194/isprs-archives-XLIII-B1-2020-507-2020

Thomas, R.G., Smith, D.G., Wood, J.M., Visser, J., Calverley-Range, E.A., and Koster, E.H. 1987. Inclined heterolithic stratification—terminology, description, interpretation and significance. Sedimentary Geology, 53:123–179. https://doi.org/10.1016/S0037-0738(87)80006-4

Thomas, R.G., Eberth, D.A., Deino, A.L., and Robinson, D. 1990. Composition, radioisotopic ages, and potential significance of an altered volcanic ash (bentonite) from the Upper Cretaceous Judith River Formation, Dinosaur Provincial Park, southern Alberta, Canada. Cretaceous Research, 11:125–162. https://doi.org/10.1016/S0195-6671(05)80030-8

Tumarkin-Deratzian, A.R. 1997. Sedimentology, taphonomy, and faunal review of a multigeneric bonebed (Bonebed 47) in the Dinosaur Park Formation (Campanian) of southern Alberta, Canada. Unpublished B.Sc. Thesis, Lafayette College, Easton, Pennsylvania, USA.

Visser, J. 1986. Sedimentology and taphonomy of a *Styracosaurus* bonebed in the Late Cretaceous Judith River Formation, Dinosaur Provincial Park, Alberta. Unpublished M.Sc. Thesis, University of Calgary, Calgary, Alberta, Canada.

Wilson, J.P., Ryan, M.J., and Evans, D.C. 2020. A new, transitional centrosaurine ceratopsid from the Upper Cretaceous Two Medicine Formation of Montana and the evolution of the '*Styracosaurus*-line' dinosaurs. Royal Society Open Science, 7:200284. https://doi.org/10.1098/rsos.200284

Wood, J.M. 1985. Sedimentology of the Late Cretaceous Judith River Formation, “Cathedral” area, Dinosaur Provincial Park, Alberta. Unpublished M.Sc. Thesis, University of Calgary, Calgary, Alberta, Canada.

Wood, J.M. 1989. Alluvial architecture of the Upper Cretaceous Judith River Formation, Dinosaur Provincial Park, Alberta, Canada. Bulletin of Canadian Petroleum Geology, 37:169–181.

Wood, J.M., Thomas, R.G., and Visser, J. 1988. Fluvial processes and vertebrate taphonomy: the Upper Cretaceous Judith River formation, south-central Dinosaur Provincial Park, Alberta, Canada. Palaeogeography, Palaeoclimatology, Palaeoecology, 66:127–143. https://doi.org/10.1016/0031-0182(88)90085-5

APPENDIX 1.

Extended Methods section with additional technical details on UAV flights, SfM photogrammetry and GIS analyses.

APPENDIX 2.

Agisoft processing report presenting technical parameters of SfM photogrammetry workflow.

APPENDIX 3.

R code to produce elevation analyses for BB190 Amphitheatre area.

APPENDIX 4.

Vertical and horizontal geographical coordinates of fossil localities and points along sedimentary unit contacts in BB190 Amphitheatre area.

APPENDIX 5.

Heights of locations of fossil specimens found in BB190 Amphitheatre area above points sampled along nearest exposure of Oldman-Dinosaur Park Formation contact.

APPENDIX 6.

Heights of locations of fossil specimens found in BB190 Amphitheatre area above nearest point sampled along base of Rhythm 4, i.e., the BB190 host horizon.

APPENDIX 7.

Vertical and horizontal geographical coordinates measured along Oldman- Dinosaur Park Formation contact exposed around Dinosaur Provincial Park public loop road (available from Currie and Koppelhus, 2005).

APPENDIX 8.

Fly-through video of a medium-resolution 3-D mesh of the BB190 Amphitheatre area.